Marine and Petroleum Geology 94 (2018) 230–245

Contents lists available at ScienceDirect

Marine and Petroleum Geology

journal homepage: www.elsevier.com/locate/marpetgeo

Research paper

# Diagenesis and evolution of the lower Eocene red-bed sandstone reservoirs in the Dongying Depression, China

Jian Wang[a,b,*], Yingchang Cao[a,b,**], Keyu Liu[a,c], Alessandra Costanzo[d], Martin Feely[d]

[a] School of Geosciences, China University of Petroleum (East China), Qingdao, 266580, China
[b] Laboratory for Marine Mineral Resources, Qingdao National Laboratory for Marine Science and Technology, Qingdao, 266071, China
[c] Department of Applied Geology, Curtin University, GPO Box U1987, Perth, WA, 6845, Australia
[d] Earth and Ocean Sciences, School of Natural Sciences, National University of Ireland, Galway, Ireland

ARTICLE INFO

*Keywords:*
Diagenesis
Diagenetic environment
Reservoir evolution
Red bed
Eocene
Dongying Depression

ABSTRACT

The diagenetic evolution of the lower Eocene red-bed high-quality reservoirs in the Dongying Depression was systematically investigated through an integrated petrographic, petrophysical, fluid evolution and thermal history analysis. The reservoirs experienced several phases of diagenesis, including compaction, carbonate cementation, gypsum and ankerite cementation, feldspar and carbonate dissolution, quartz overgrowth cementation, and clay-mineral cementation and transformation. An early alkaline diagenetic environment caused significant cementation of calcite and gypsum in the reservoir sandstone units near the sandstone-mudstone contacts. Acidic formation fluids caused widespread dissolution of the feldspar and carbonate cements, leading to synchronous occurrences of primary intergranular pores and acidic dissolution pores. From the middle parts of the reservoir sandstone units to the sandstone-mudstone contacts, dissolution wanes gradually with ferro-carbonate progressively diminishing. Migration of exogenetic thermal fluid along faults may have contributed to the gradual decrease in dissolution and the gradual increase in cementation from the lower part to the upper part of fault blocks. The alternating alkaline and acidic diagenetic environments and the distribution of diagenetic products caused the development of the high-quality red-bed reservoirs in the middle part of the thick-layered sandstone units in the lower part of fault blocks. Because of the spatial and temporal relationships between the diagenetic stages and their products, lithological traps of a diagenetic origin were developed in the red-bed reservoirs.

## 1. Introduction

Red beds are unique detrital sedimentary rocks with a singular color of reddish–brown, caused by ferric oxide pigments on grains, filling pores, or dispersed in clay matrix (van Houten, 1973; Walker, 1974). Geological research on red beds dates back to the early 19th century, and focused primarily on aspects of their mineralogy and petrology, paleomagnetism, paleoclimate and paleontology. The geochemical effects of trace minerals in red beds, such as biotite and hematite, during the diagenetic process were also investigated to elucidate the causes of reddish color (Turner and Archer, 1977; Walker, 1967, 1976; 1981; Parcerisa et al., 2006). Paleomagnetism of red beds was used to reconstruct tectonic evolution by measuring residual magnetism in red beds (Kent and Opdyke, 1978; Yamashita et al., 2011). The occurrence of red beds had once been widely considered as direct indicators for arid palaeoclimatic settings related to desert or savanna, with assumptions that red soil might supply red alluvium, and that reddish–brown hydrated ferric oxides might not be converted to hematite at surface conditions (van Houten, 1973). However, numerous studies question these assumptions and therefore strongly oppose the view that red beds only indicate arid climate conditions (Turner, 1980; Sheldon, 2005). The occurrence of ferric oxides, mainly in the form of hematite in red beds, do not have climatic significance (van Houten, 1973; Turner, 1980; Sheldon, 2005). To date, generic continental red beds have been reported from environments and climatic settings of humid tropics (Walker, 1974; Besly and Turner, 1983), temperate monsoon (Dubiel and Smoot, 1994), (sub-)tropical monsoon (Retallack, 1991), as well as desert and savanna (Walker, 1976). Palaeo-environment changes were also deduced from the fossils in red beds (Marriott et al., 2009). In China, widely distributed red beds occur as outcrops and sedimentary strata in sedimentary basins, which are composed of continental clastic sediments formed in arid climatic conditions.

* Corresponding author. School of Geosciences, China University of Petroleum, Qingdao, Shandong, 266580, China.
** Corresponding author. School of Geosciences, China University of Petroleum, Qingdao, Shandong, 266580, China.
*E-mail addresses:* wangjian8601@upc.edu.cn (J. Wang), caoych@upc.edu.cn (Y. Cao).

https://doi.org/10.1016/j.marpetgeo.2018.04.011
Received 24 September 2017; Received in revised form 11 April 2018; Accepted 12 April 2018
Available online 13 April 2018

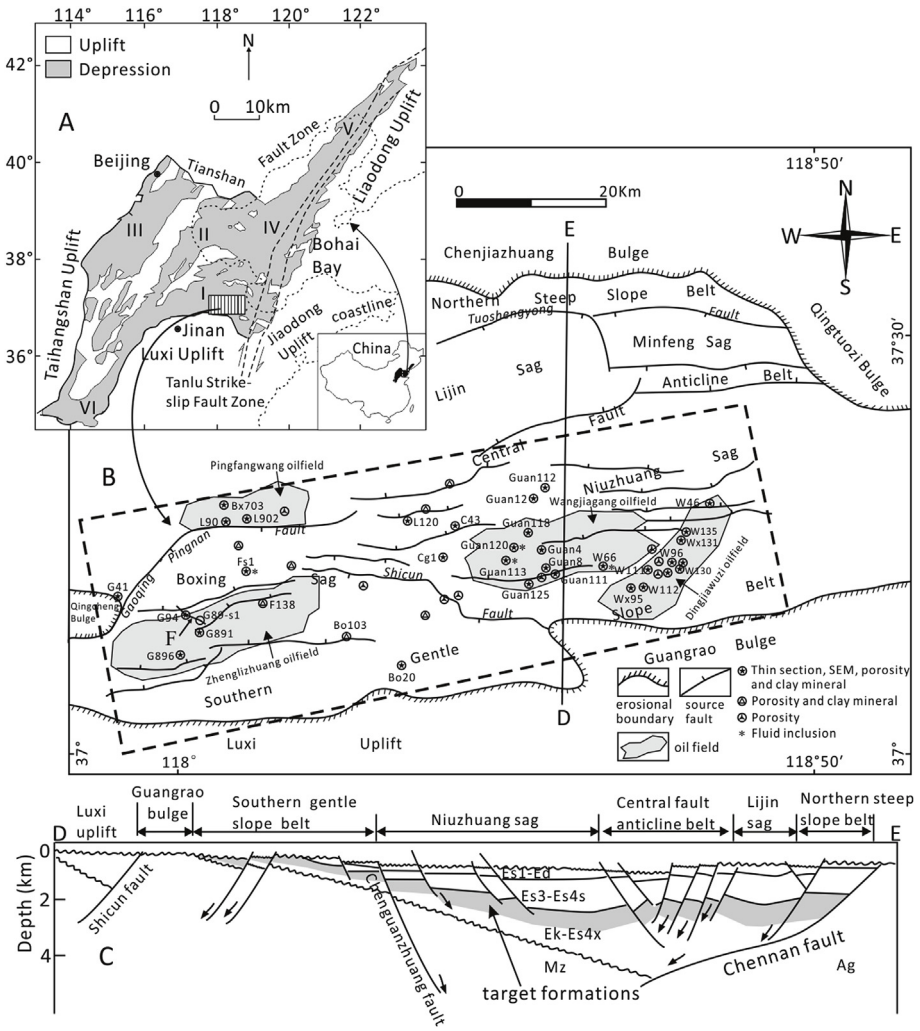


**Fig. 1.** (A) Tectonic setting of the Dongying Depression in the southern Jiyang subbasin (I) of the Bohai Bay basin. Other subbasins in Bohai Bay basin are Huanghua subbasin (II), Jizhong subbasin (III), Linqing subbasin (IV), Bozhong subbasin (V) and Liaohe subbasin (VI). (B) Structural map of the Dongying depression with well locations, main faults and oil fields of the *Ek1-Es4x*. (C) Section structural characteristics and target formations of the Dongying depression. (F) Location for cross section of Fig. 18.

Influenced by seasonal inflowing water, red beds in basins of East China usually occur as alternated sandstone and mudstone intervals (Wang et al., 2015). Under an arid climatic setting, the palaeo-salinity levels in lake waters were relatively high, often causing evaporites being deposited in the sag belts of basins (Wang et al., 2015; Liu et al., 2017).

Red-bed sandstone reservoirs have recently become an important exploration target in the Bohai Bay Basin (Wei and Yuan, 2008; Wang et al., 2015, Fig. 1A). The early exploration results indicate that the red beds of the first member of the Kongdian Formation (*Ek1*) and lower fourth member of the Shahejie Formation (*Es4x*) are important exploration target reservoir intervals in the Dongying Depression (Fig. 2). Since 2006, four oil fields have been discovered in the two red-bed reservoir intervals, including the Zhenglizhuang (2950–4150 m), Pingfangwang (1800–3250 m), Wangjiagang (2000–3650 m), and Dingjiawuzi (1300–3500 m) oil fields (Fig. 1B). Such discoveries show an enormous exploration potential of the red-bed sandstone reservoirs in the Dongying Depression. The dark mudstone of the top part of the upper fourth member of the Shahejie Formation*(Es4s)*immediately above *Es4x* not only provided considerable hydrocarbons to red-bed sandstones by lateral connection through faults but also act as a good top seal for the red-bed reservoirs (Jiang et al., 2011). Because of the favorable combinations of the hydrocarbon source, reservoir and seal, the red-bed sandstones are considered to be the favored exploration targets in the Dongying Depression.

Sedimentation controls the initial porosity and influences the diagenesis of the reservoirs to a certain degree (Aagaard and Jahren, 2010; Hammer et al., 2010). Diagenesis is the dominant factor in the evolution of the porosity of clastic reservoirs during the burial process (Schmid et al., 2004; Al Gahtani, 2013; Nguyen et al., 2013; Wilson et al., 2013; Henares et al., 2014). A series of ordered stacking diagenetic events occurred during the evolution of diagenetic environments; these events controlled the diagenetic transformation process, formed the present diagenetic appearance and reservoir features (Li et al., 2006). Compared with the study of depositional characteristics of the sandstones, the study of diagenesis and its influence on reservoirs is rather limited in scope (Dill et al., 2005; Schoner and Gaupp, 2005; Parcerisa et al., 2006). In this study, we investigated the characteristics of diagenesis, diagenetic environments and diagenetic evolution and the causes for the development of high-quality reservoirs of red-bed reservoirs in the Dongying Depression using an integrated petrographic, petrophysical, fluid evolution and burial history analysis.

## 2. Geological background

The Bohai Bay Basin is an important hydrocarbon producing basin that is located on the eastern coast of China and covers an area of

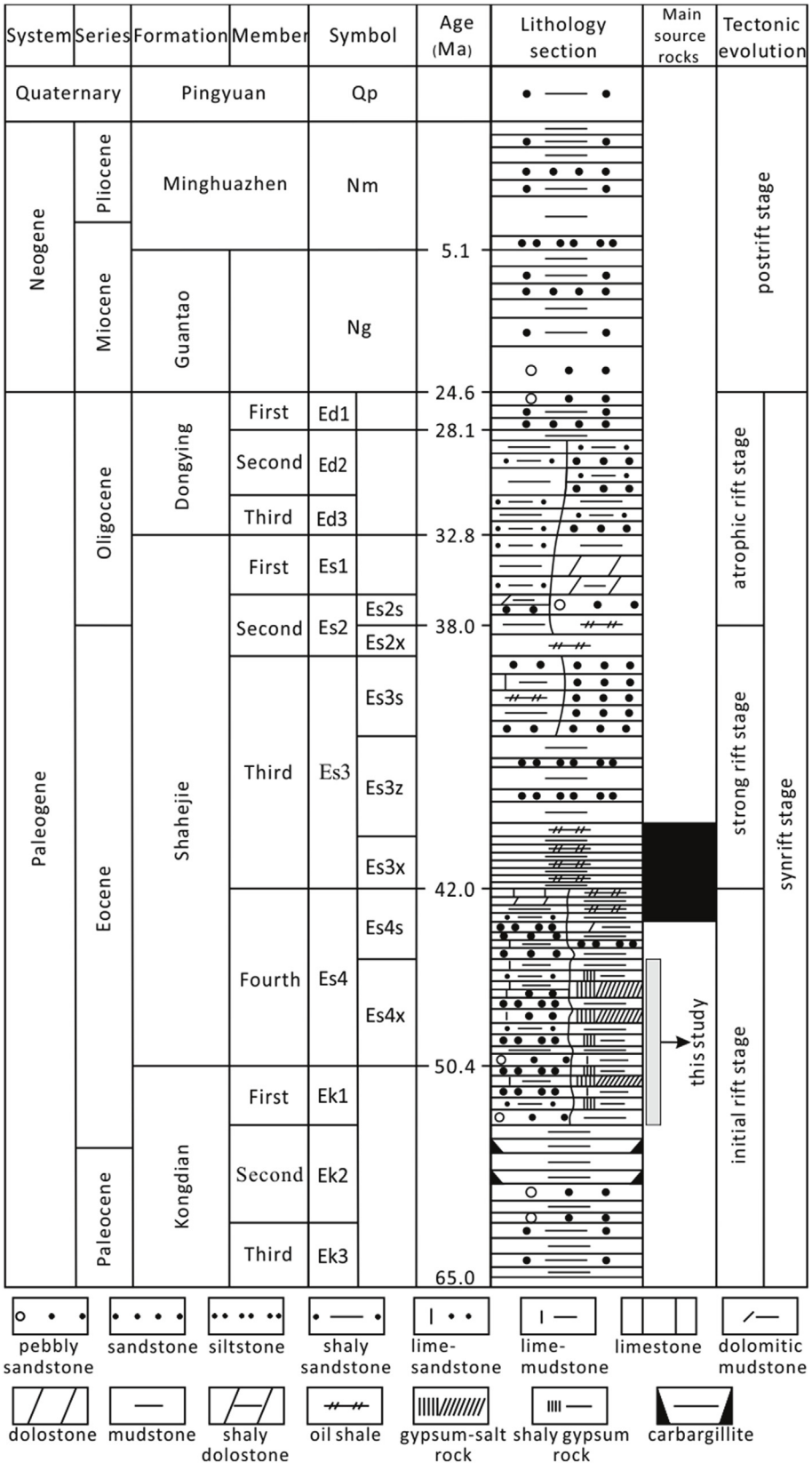


**Fig. 2.** Schematic Tertiary stratigraphy and tectonic evolution of the Dongying Depression. Ek1-Es4x formations developed at the initial rift stage and were comprised of sandstones interbedded with mudstones in southern and gypsum-salt deposits in the northern Dongying Depression. *QP*-Quaternary Pingyuan formation; *Nm*-Neocene Minghuazhen formation; *Ng*-Neocene Guantao formation; *Ed1*-The first member of Paleogene Dongying formation (*Ed*); *Ed2*-The second member of *Ed*; *Ed3*-The third member of *Ed*; *Es1*-The first member of Paleogene Shahejie formation (*Es*); *Es2s*-The upper second member of *Es*; *Es2x*-The lower second member of *Es*; *Es3s*-The upper third member of *Es*; *Es3z*-The middle third member of *Es*; *Es3x*-The lower third member of *Es*; *Es4s*-The upper fourth member of *Es*; *Es4x*-The lower fourth member of *Es*; *Ek1*-The first member of Paleogene Kongdian formation (*Ek*); *Ek2*-The second member of *Ek*; *Ek3*-The third member of *Ek*.

approximately 200,000 km$^2$. The basin is a complex rifted basin that formed in the Late Jurassic through the early Tertiary on the basement of the North China platform. The tectonic evolution of the basin consists of a synrift stage (65.0–24.6 Ma) and postrift stage (24.6 Ma to present) (Lampe et al., 2012). The Bohai Bay Basin consists of several subbasins (Fig. 1A). The Dongying Depression is a secondary tectonic unit of the Jiyang subbasin in Shandong Province, comprising the Qingtuozi Bulge in the east, Guangrao Bulge in the southeast, Luxi Uplift in the south, Qingcheng Bulge in the west and Chenguangzhuang Bulge in the north (Fig. 1B). Based on its tectonic characteristics, the Dongying Depression

can be divided into five tectonic belts from north to south: the northern steep slope belt, northern sag belt, central fault anticline belt, southern sag belt and southern gentle slope belt (Fig. 1C).

The depression is filled with Cenozoic sediments, comprising the Paleogene Kongdian (*Ek*), Shahejie (*Es*) and Dongying (*Ed*) formations, Neogene Guantao (*Ng*) and Minghuazhen (*Nm*) formations and Quaternary Pingyuan (*Qp*) Formation (Fig. 2). The development of the synrift basin, which was influenced by the Himalayan movement, experienced three stages: initial rift stage, strong rift stage and atrophic rift stage (Feng et al., 2013). The red beds were uplifted at the end of the *Ed* Formation and experienced some subsidence during the deposition of the *Nm* Formation, influenced by the regional tectonic movement (Lampe et al., 2012).

East Asian Paleogene climates have long been regarded as being controlled by the planetary wind system, which results in a climate pattern with three latitudinally distributed zones. Two humid zones located separately in the north and south, characterized lithologically by coals and oil shales, while an arid zone in the middle was represented by red beds and evaporites (Quan et al., 2014). The study area is located at the border of the arid zone and the north humid zone. During the deposition of the Eocene *Ek1-Es4x* formations, because of frequent alternations between dry and wet climates under an arid climatic setting and a gentle paleogeomorphology, the evaporitic lake of the early Eocene Dongying Depression experienced frequent lake-level and salinity oscillations (Wang et al., 2015). Thick and widespread gray, gray-green and red sandstones interbedded with red and gray-green mudstones in the southern Dongying Depression and gypsum-salt deposits in the northern sag belt were developed (Liu et al., 2017). The frequently interbeds of sandstones with purplish-red mudstones on cores indicates an arid-semi-arid climate and that the facies of the red beds are dominated by distributary channels in over-flooding lake deltas (Wang et al., 2015; Liu et al., 2017). Formations of *Ek1-Es4x* in the southern Dongying Depression are divided into numerous fault blocks by some large oil source-connecting faults in a downdip direction and antithetic faults in an updip direction.

## 3. Methodology

Core samples of red-bed sandstone were collected from 46 wells in the study area (Fig. 1B). Samples were impregnated with blue resin before thin sectioning in order to highlight pores. Thin sections were partly stained with Alizarin Red S and K-ferricyanide for carbonate mineral determination. The discrimination of quartz and feldspar is through optical microscopy. Petrographic point counting was performed on 143 thin sections by counting 300 points per thin section to identify mineral compositions and pores. The Udden-Wentworth grain size scale (Udden, 1914; Wentworth, 1922) was used and sorting ranking was determined in accordance with the standard charts of Folk (1974).

A total of 316 samples were collected for mineralogical analyses using X-ray diffraction (XRD). A D8 DISCOVER was used for XRD analysis with Cu-Ka radiation, a voltage of 40 kV, and a current of 25 mA. Prior to analysis each sample was oven-dried at 40 °C for 2 days and ground to < 40 μm using an agate mortar to thoroughly disperse the minerals. In order to analyze the compositions of clay minerals, the samples were put in a plastic bottle, soaked in distilled water, and then disintegrated with an oscillator. Distilled water was added to the sample until the conductivity is less than 50 μs, and the suspension was separated by a centrifuge at a speed of 2000 r/min for 2 min. Filtering granular suspension less than 2 μm with ceramic filter, and then the clay mineral particles were placed in an oven to dry at 50 °C. No chemical pre-treatment was employed. Samples were scanned from 3° to 70° with a step size of 0.02°. Analysis of the XRD data provides relative abundances (in weight percent) of the various clay mineral phases. Eight samples were analyzed using a Hitachi S-4800 scanning electron microscopy under the conditions of 20 °C, 35%RH, and 5.0 kV.

Porosity was measured from core plugs of 2.5 cm in diameter using on a helium porosimeter following Boyle's law. Dry, clean core samples were placed in a porosimeter and injected with helium at approximately 200 psi. Corresponding pressures and volumes were measured and utilized in the Boyle's Law equation to calculate sample grain volume. Pore volumes were determined by subtracting the grain volumes from the measured bulk volumes, and the total porosity was then calculated from the grain and bulk volumes.

Four representative samples from four wells (Well Fs-1, 3584.2 m; Guan-120, 2945.75 m; Guan-113, 2494.49 m; W-66, 2200.3 m, respectively) were prepared as doubly polished fluid-inclusion wafers and analyzed by microthermometry at the Geofluids Research Laboratory of Earth and Ocean Sciences, National University of Ireland Galway. The selection of samples mainly considered the area, depth and the abundance of fluid inclusions in cements. The four samples selected are thought to represent the whole depth range of the entire formation and the west, middle and east part of study area. Fluid inclusions are quite abundant in quartz overgrowth, annealed microfractures (AMF) and carbonate cements in the four samples and are informative for the study of fluid evolution during reservoir diagenesis. Microthermometry was conducted using a Linkam Scientific THMSG-600 Geology System heating-freezing stage. Calibration of the stage was performed following the method outlined by MacDonald and Spooner (1981); in addition, synthetic fluid inclusion standards were used (pure $CO_2$ and water). The precision was ± 0.2 °C at −56.5 °C and ± 2 °C at 300 °C. The eutectic temperatures ($T_e$), last ice melting temperatures ($T_{mice}$), and homogenization temperatures ($T_h$) were observed at a heating rate of up to 5 °C/min.

## 4. Results

### 4.1. Petrological compositions of red-bed sandstones

The compositions of red-bed sandstones are summarized in Table 1. The detrital compositions red-bed sandstones are mainly lithic arkoses according to Folk (1980) classification scheme, with corresponding average compositions being $Q_{42.5}F_{33.2}R_{24.3}$. There is no obviously difference of detrital compositions between sandstones less than 1 m and sandstones more than 1 m to the sandstone-mudstone contacts (Table 1). The detrital quartz is the highest component among all samples analyzed. Detrital feldspars comprise both K-feldspar and plagioclase. Lithic fragments are mainly of volcanic and metamorphic types, with a small amounts of sedimentary in origin. Other detrital components include mainly small amounts of mica (Table 1). The interstitial materials of the red-bed sandstones consist mainly of clay matrix and cements. The cements are dominated by carbonates including calcite, dolomite, ferro-calcite and ankerite with a minor amount of quartz overgrowths and clay minerals (Table 1). The sorting ranges from well (1.2) to poorly (3.92) sorted.

### 4.2. Reservoir diagenetic types and characteristics

#### 4.2.1. Compaction

Because the burial depth of red-bed reservoirs spans over a wide range, there are significant differences in compaction in different depth ranges. For example, the burial depth in the reservoirs of Well W-96 is generally 1800–2300 m, and the grains are primarily of point contact or line contact; for the reservoirs of Well Fs-1 and Well G-94, however, the burial depth is generally greater than 3500 m, and the grains generally exhibit line contact and concave-convex contact or even suture contact. In some areas, rigid particles of the feldspar and quartz are subject to crushing and fracturing (Fig. 3A). The original porosity destroyed by compaction is in a relatively large range at the same depth. In order to analyze the influence of compaction on reservoir porosity quantitatively, the original porosity destroyed by compaction was calculated by the Equation of Wang et al. (2017a). The $V_{initial}$ was established by

**Table 1**
The petrological compositions of the red-bed sandstones in the Dongying Depression.

| | Less than 1 m to the sandstone-mudstone contact | | | More than 1 m to the sandstone-mudstone contact | | |
|---|---|---|---|---|---|---|
| | Min | Max | Mean | Min | Max | Mean |
| Detrital grains | | | | | | |
| Quartz (vol. %) | 33.3 | 54.6 | 42.1 | 34.7 | 55.5 | 42.9 |
| Potassium feldspars (vol. %) | 10.2 | 22 | 15.9 | 10 | 22 | 15.7 |
| Plagioclase feldspars (vol. %) | 15 | 22.1 | 17.2 | 15.6 | 22.5 | 17.6 |
| Volcanic lithic fragments (vol. %) | 0.7 | 34.2 | 5.9 | 0.7 | 35 | 6.7 |
| Metamorphic lithic fragments (vol. %) | 5.4 | 30.1 | 12.5 | 5 | 30.7 | 11.9 |
| Sedimentary lithic fragments (vol. %) | 0 | 17.4 | 4.8 | 0 | 18 | 5.4 |
| Mica (vol. %) | 0.2 | 4.3 | 0.8 | 0 | 4.3 | 0.6 |
| Diagenetic alterations | | | | | | |
| Calcite (vol. %) | 9 | 22.2 | 12.6 | 1.3 | 10 | 1.8 |
| Ferrocalcite (vol. %) | 0.5 | 6 | 1.8 | 1.2 | 6.4 | 2.4 |
| Dolomite (vol. %) | 0 | 6 | 0.7 | 0 | 7.7 | 0.9 |
| Ankerite (vol. %) | 0 | 2 | 0.2 | 0 | 3 | 0.6 |
| Gypsum and Anhydrite (vol. %) | 0 | 23 | 3.3 | 0 | 3 | 0.1 |
| Quartz overgrowth (vol. %) | 0 | 0.5 | 0.2 | 0.05 | 1.2 | 0.6 |
| Pyrite (vol. %) | 0 | 4.4 | 0.6 | 0 | 4.7 | 0.8 |
| Clay matrix (vol. %) | 0 | 16 | 7.2 | 1.7 | 14.2 | 6.4 |
| Kaolinite (%) | 0 | 22 | 3.3 | 2 | 56 | 24.6 |
| Illite (%) | 0 | 18.2 | 3.1 | 1.7 | 38.3 | 23.4 |
| Illite-smectite mixed layers (%) | 0 | 29.1 | 3.7 | 3.7 | 69.3 | 45.6 |
| Chlorite (%) | 0 | 8.5 | 2.5 | 3 | 28.3 | 13.1 |
| Porosity | | | | | | |
| Intergranular porosity (%) | 0 | 10 | 1.3 | 0.6 | 17.9 | 6.4 |
| Intargranular porosity (%) | 0.03 | 1.3 | 0.4 | 0.04 | 1.7 | 0.9 |
| Dissolution porosity (%) | 0.03 | 2 | 0.5 | 0.04 | 2.3 | 1.2 |

Note: The volume of detrital grains by point counting refers to the total framework composition. The volume of diagenetic minerals, clay matrix and porosity by point counting refer to the total composition. The content of clay minerals by XRD refers to the total clay content.

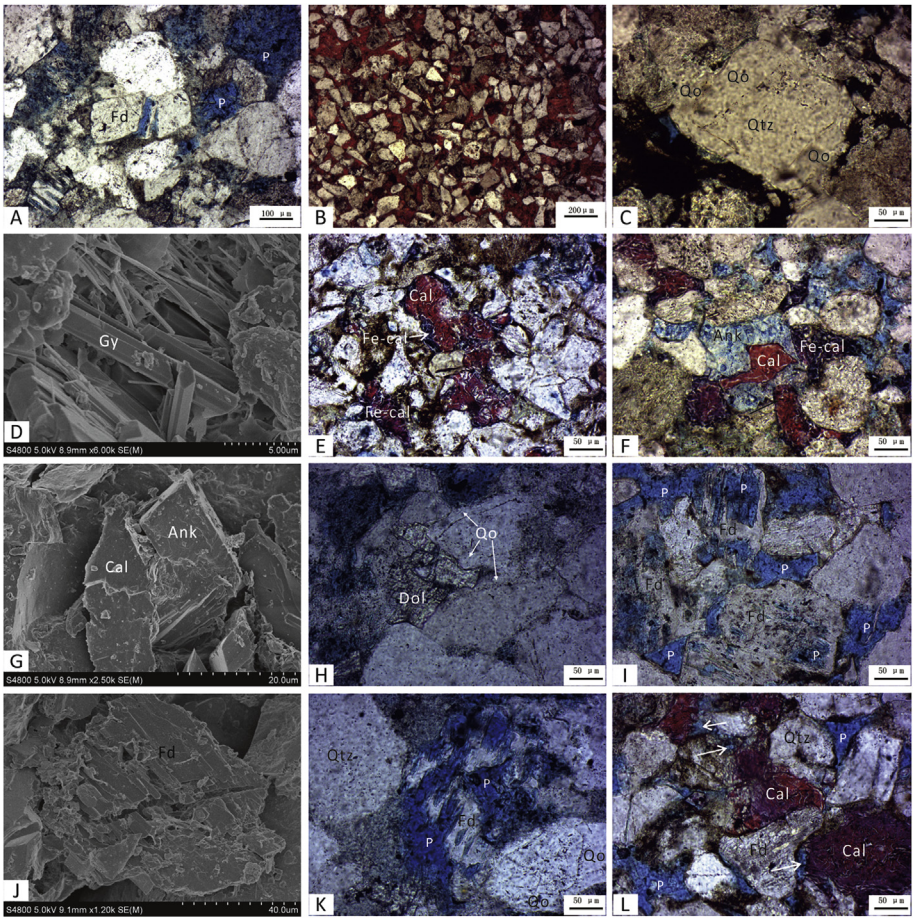


**Fig. 3.** Photos from thin sections and scanning electron microscopy show types of diagenesis of red-bed reservoirs of the lower Eocene *Ek1-Es4x* in the Dongying Depression. (A) Feldspar compaction fracture (−) from Well L-902 at 2532.45 m, *Ek1*; (B) Strong calcite cementation (−) from Well Wx-99 at 2093.04 m, *Ek1*; (C) Quartz overgrowth cementation (−) from Well Fs-1 at 3584.2 m, *Ek1*; (D) Gypsum cementation from well Guan-120 at 2950.09 m, *Es4x*; (E) Calcite and ferrocalcite cementation (arrow) (−) from Well Guan-118 at 3007.7 m, *Es4x*; (F) Isolated calcite, ferro-calcite and ankerite cements filled in intergranular pores, and grains are in point-line contact (−) from Well G-891, 2808.4 m, *Es4x*; (G) Calcite and ankerite cementation from Well Guan-4 at 2749.7 m, *Es4x*; (H) Dolomite and quartz overgrowth from Well Guan-4 at 2749.7 m, *Es4x*; (I) Dissolution of feldspar (−) from Well W-130 at 2182.3 m, *Ek1*; (J) Dissolution of feldspar from Well Guan-113 at 2494.49 m, *Ek1*; (K) Dissolution of feldspar and quartz overgrowth cementation (−) from Well L-902 at 2532.45 m, *Ek1*; (L) Dissolution of carbonate cements (arrows) (−) from Well W-130 at 2081.4 m, *Ek1*. Qtz-quartz; Fd-feldspar; Cal-calcite; Fe-cal-ferro-calcite; Qo-quartz overgrowth; Dol-dolomite; Ank-ankerite; Gy-gypsumP-pores. (−) indicates polarized light. See Fig. 1B for well locations.

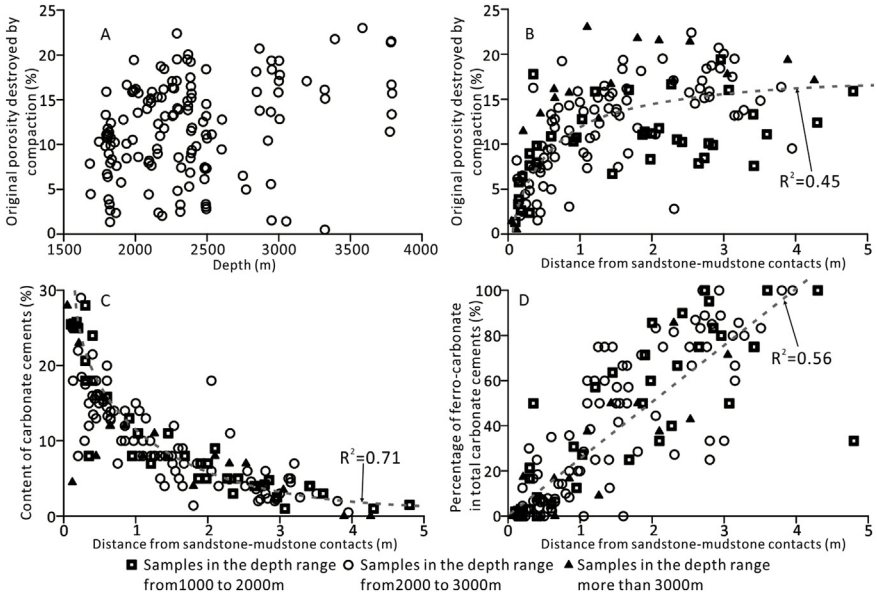


**Fig. 4.** (A) Relationship between original porosity destroyed by compaction and depth; (B) Relationship between original porosity destroyed by compaction and distance from sandstone-mudstone contacts; (C) Relationship between content of carbonate cements and distance from sandstone-mudstone contacts; (D) Relationship between relative content of ferro-carbonate cements and distance from sandstone-mudstone contacts.

using Beard and Weyl's method (1973). The samples with more than 5% matrix were excluded during the calculation in order to avoid overestimation of the compaction (Paxton et al., 2002).

$$V_{compaction} = V_{initial} + V_{dissolution} - V_{cementation} - V_{present} \quad (1)$$

$V_{initial}$-initial pore volume; $V_{compaction}$-pore volume destroyed by compaction; $V_{dissolution}$-dissolution pore volume; $V_{present}$-present pore volume.

$$V_{initial} = 20.91 + (22.9/So) \quad (2)$$

*4.2.1.1. So-sorting coefficient.* With increasing burial depth, the original porosity destroyed by compaction has no obviously change (Fig. 4A). In different burial depth ranges (1000–2000 m, 2000–3000 m, > 3000 m) the original porosity destroyed by compaction shows a similar increase from the sandstone-mudstone contacts to the middle of the sandstone units (Fig. 4B). Within a distance of less than 1 m from the sandstone-mudstone contacts, the original porosity destroyed by compaction is usually less than 15%. When the distance is more than 1 m from the sandstone-mudstone contacts, the original porosity destroyed by compaction is generally between 10% and 25% (Fig. 4B).

*4.2.2. Cementation*

The cements in the red-bed reservoirs primarily include carbonate, silica, sulfate, and clay minerals (Table 1; Fig. 3B, C, D, E, F, G, K and L). Carbonate cement is the dominant type of cement and includes calcite, ferro-calcite, dolomite and ankerite (Table 1); the content is generally 2.3–30% with an average of 10.5%. The high carbonate cement content zone is in the depth range of 1500–2500 m (Fig. 5). Calcite is the dominant carbonate cement. The content of calcite within 1 m to the sandstone-mudstone contacts is 9%–22.2% with an average of 12.6%; beyond 1 m to the sandstone-mudstone contacts, the content of calcite reduces sharply to 1.3%–10% with an average of 1.8% (Table 1). There are two types of calcite cements in red-bed sandstone reservoirs. The first type fills all the intergranular pores as crystalline calcite cements. The clastic grains mainly occur as point contacts (Fig. 3B). This illustrates that the precipitation was earlier, the cement content is higher and reservoir is more tightly cemented. The second type occurs as isolated calcite cement filling some intergranular pores. The clastic grains have point-line contacts between each other, and cement content is relatively lower (Fig. 3E, F and L). Dolomite mainly occurs as isolated cements filling some intergranular pores (Fig. 3H). The content of dolomite is generally less than 8% with an average of 0.8%. There is no obvious difference in dolomite content between sandstones less than 1 m and more than 1 m to the sandstone-mudstone contacts (Table 1). The content of dolomite appears to become relatively high only in some depth ranges (Fig. 5). Ferro-calcite cements usually occur around the isolated calcite cements or as isolated cement-filling pores (Fig. 3E and L). The content of ferro-calcite is usually less than 8% with an average of 2.1%. The high contents of ferro-calcite occur in the depth range of 2000–3000 m (Fig. 5). Ankerite cements generally appear in intergranular pores (Fig. 3F). The content of ankerite is usually less than 6% with an average of 0.4%. Ankerite occurs mainly in depth ranges over 3250 m (Fig. 5). The contents of ferro-calcite and ankerite within 1 m to sandstone-mudstone contacts are slightly higher than that beyond 1 m to sandstone-mudstone contacts (Table 1).

Siliceous cements primarily occur as quartz overgrowths. Most samples display singular quartz overgrowth, but some samples record two overgrowth stages (Fig. 3C, H and K). The amount of quartz overgrowth is usually 0.05%–1.2% with an average of 0.4%. The content of quartz overgrowth within 1 m to the sandstone-mudstone contacts is higher than that beyond 1 m to the sandstone-mudstone contacts (Table 1). Between 1500 m and 2500 m depth range the content of authigenic quartz is relatively high (Fig. 5).

The carbonate cement content decreases from the sandstone-mudstone contacts to the middle of the sandstone units at different burial depth ranges (Fig. 4C). Within 1 m to the sandstone-mudstone contacts, the carbonate cement content rapidly decreases; beyond 1 m from the sandstone-mudstone contacts, the carbonate cement content declines slowly. The ferro-carbonate content is relatively low (Table 1), whereas its percentage gradually increases from the sandstone-mudstone contacts to the middle of sandstone units at different burial depth ranges (Fig. 4D). The crystalline calcite and gypsum/anhydrite cementation are often observed in sandstones near the sandstone-mudstone contacts with clastic grains mainly being of point contact. The middle of sandstone units have a low cement content, abundant intergranular pores and relatively high porosity (Fig. 6). It is clear from the COPL-CEPL diagram (Lundegard, 1992) that the majority of samples within 1 m to the sandstone-mudstone contacts have lost more porosity by cementation than by compaction, while the majority of samples beyond 1 m to the sandstone-mudstone contacts have lost more porosity by compaction than by cementation (Fig. 7). The negative relationship between the original porosity destroyed by cementation and the original porosity destroyed by compaction indicates that cementation prevented

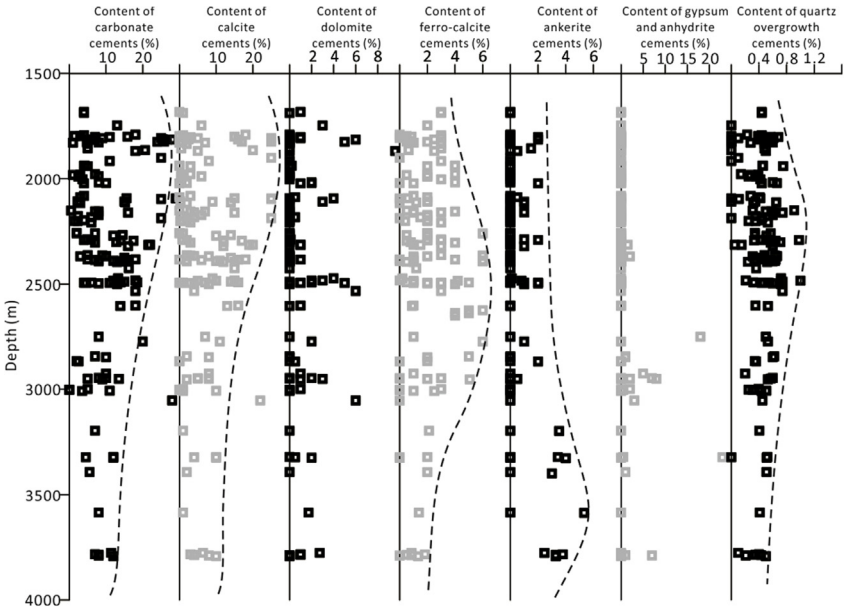


**Fig. 5.** Content and vertical distribution of carbonate cements, sulfate cements and quartz overgrowth cements of red-bed reservoirs of the lower Eocene *Ek1-Es4x* in the Dongying Depression. The results of content of cements are from point counting based on the total modal composition.

compaction to some extent (Fig. 7).

Inside the fault block, the carbonate cement contents also decrease gradually from the sandstone-mudstone contacts to the middle of the sandstone units at different distance ranges to the oil source-connecting faults (Fig. 8A). The quartz overgrowth contents increase gradually from the sandstone-mudstone contacts to the middle of the sandstone units at different distance ranges to the oil source-connecting faults (Fig. 8B). There is no obvious relationship between the content of carbonate cements and quartz overgrowths and the distance from the faults within 1 m to the sandstone-mudstone contacts (Fig. 8A and B). Beyond 1 m, the carbonate cement content is relatively low and has a positive relationship with the distance from the faults (Fig. 8A); the quartz overgrowth content is relatively high and also has a positive relationship with the distance from the faults (Fig. 8B).

Sulfate cements are dominated by gypsum and anhydrite and are primarily distributed in the well districts of Guan-4 and L-120. The sulfate cements fill both primary and secondary pores, and the content is generally of 0–23%. Cryptocrystalline hematite is the main cause of the red color for the red-bed reservoirs, and is often observed in thin sections of sandstone (Jiang and Liu, 2011).

The red-bed sandstone contains numerous clay minerals (including matrix material and authigenic clay minerals) volumetrically up to 16% (Table 1). The main component of the clay cement as revealed by XRD and SEM analyses is kaolinite, illite, chlorite and illite-smectite mixed layer (Figs. 9 and 10). Kaolinite is characterized by well-crystallized, pseudohexagonal platelets, and vermicular or booklet texture, both occurring as pore-filling cement (Fig. 9A and B). Authigenic hair-like or sheet-like illite occurs in most samples and often grows on pore spaces (Fig. 9C). The illite-smectite mixed layer is commonly sheet-like or flake-like, occurring as pore-lining rims and pore filing cement (Fig. 9D, E and F). Chlorite typically grows on the surface of detrital grains (Fig. 9F).

The clay minerals in the red-bed sandstone reservoirs are classified into two vertical transformation zones (Fig. 10). Within the burial depth

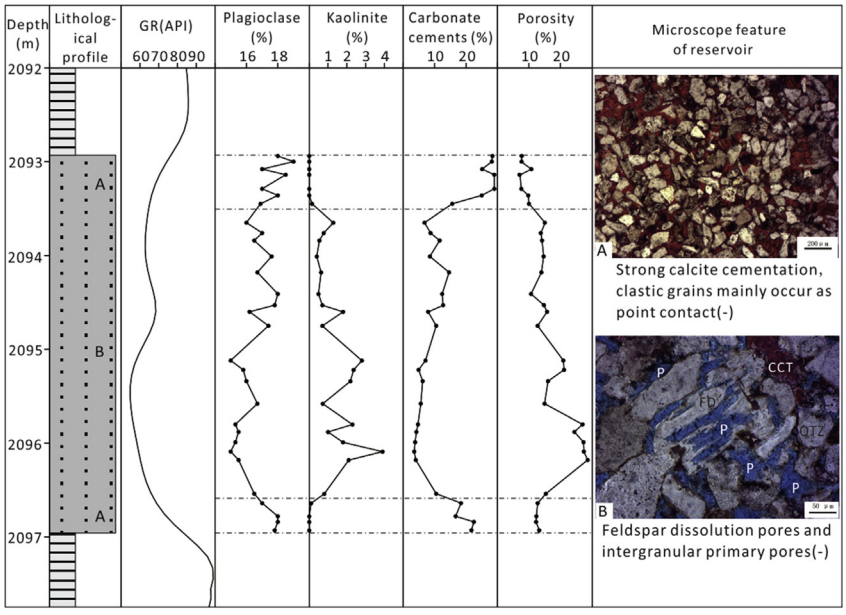


**Fig. 6.** Characteristics of porosity, cementation and dissolution in different positions of sandstones interbedded with mudstones (Well Wx-99). (A) At the boundary of sandstones, strong calcite cementation, point contacts mainly occur between clastic grains, porosities are low and increase from sandstone-mudstone contact to center. (B) In the middle part of sandstones, porosities are high with feldspar dissolution and authigenic kaolinite. (−) indicates plane polarized light.

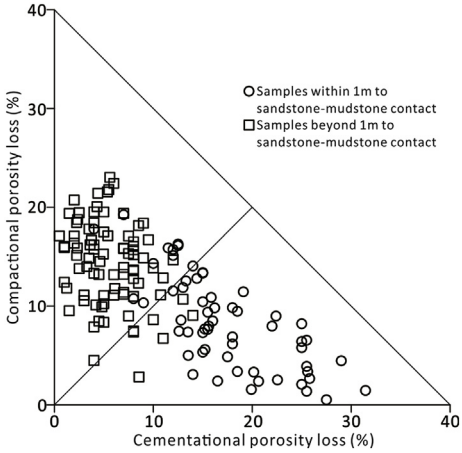


**Fig. 7.** Cross plot of compactional porosity loss versus cementational porosity loss for the red-bed sandstones.

range of 1600–2300 m, clay minerals are composed mainly of kaolinite and illite-smectite mixed layer. The percentage of kaolinite is up to 60%, the percentage of illite-smectite mixed layer is between 20% and 80% with the ratio of I-S in the range of 20% and 70% (Fig. 10), indicating that the illite-smectite mixed layer is chaotic. Within the depth range of 2300–4000 m, the percentage of illite and chlorite are obviously increased, the percentage of kaolinite and illite-smectite mixed layer are apparently reduced, and the ratio of I-S is mainly 20% (Fig. 10), indicating the illite-smectite mixed layer is orderly. There is an absence of kaolinite in sandstones near the sandstone-mudstone contacts. The contents of clay minerals within 1 m to the sandstone-mudstone contacts are obviously lower than that beyond 1 m to the sandstone-mudstone contacts (Table 1 and Fig. 6).

The content of clay minerals in mudstones is slightly higher than that in sandstones. In the burial depth range less than 2250 m, the percentage of kaolinite and illite-smectite mixed layer in mudstones are lower than that in sandstones; in the depth range of more than 2250 m, the percentage of these clay minerals in mudstones is similar to that in sandstones. The percentage of chlorite in mudstones is higher than that in sandstones, and percentage of illite and the ratio of I-S in mudstones is similar to that in sandstones.

Other diagenetic phenomena, including (1) carbonate mineral replacement of detrital grains and other cements, e.g. ferrocalcite and ankerite replacing quartz overgrowths as well as quartz and feldspar grains (Fig. 3E, F and L); (2) ferrocalcite and ankerite replacement of calcite (Fig. 3E and F). The replacement reflects the sequence of formation of the authigenic minerals in the reservoirs (Morad et al., 2012; Henares et al., 2014).

#### 4.2.3. Dissolution

Optical microscopy and SEM analyses indicate that dissolution of feldspar and carbonate cements is common in the red-bed sandstone reservoirs (Fig. 3 H, I, J, K and L and Fig. 9A). Based on thin section textures, the visual dissolution porosity is generally 0.03–2.3%, while the visual intergranular porosity is generally 0–17.9%. The percentage of the feldspar dissolution porosity accounts for over 75% of the total dissolution porosity, while the percentage of the carbonate cement dissolution porosity is less than 25%. The visual dissolution porosity has a positive correlation with the visual intergranular porosity and the measured porosity (Fig. 11).

Dissolution is primarily developed in the center of sandstones, where abundant feldspar dissolution pores are usually present with authigenic kaolinite (Fig. 6B). Dissolution porosity gradually increases from sandstone-mudstone contacts to the center of sandstones at all depth ranges (Fig. 8C), which is consistent with the spatial trend of measured porosity from sandstone-mudstone contacts to the center of

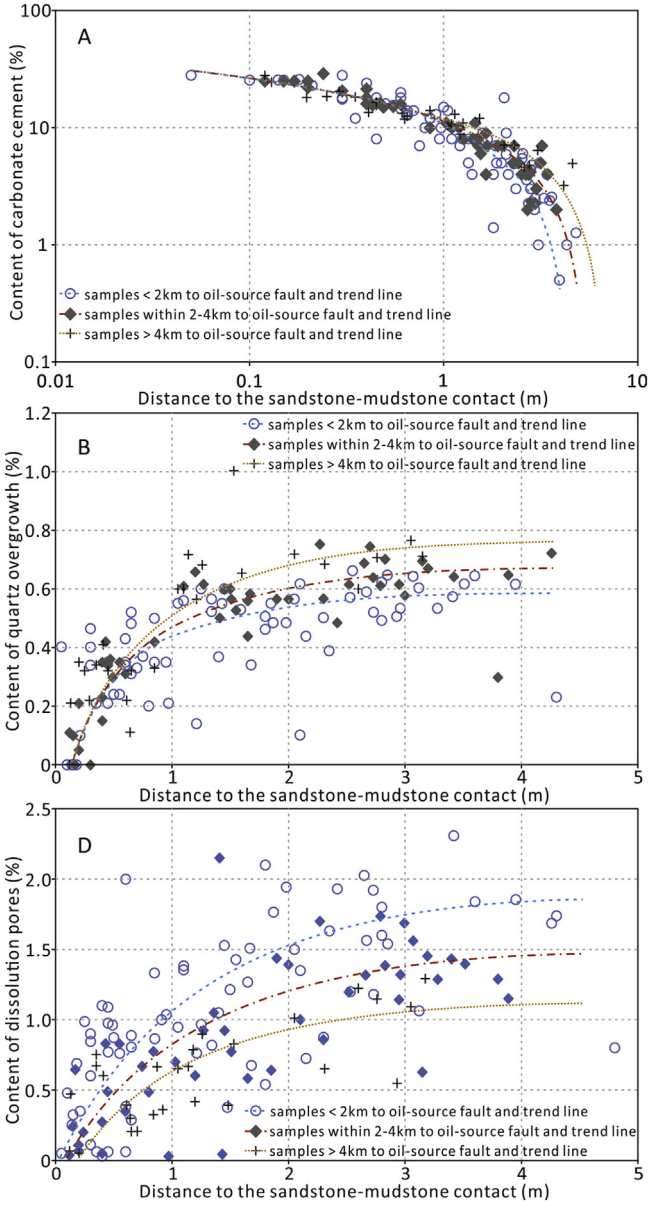


**Fig. 8.** Distribution of carbonate cement, quartz overgrowth and dissolution pores from the sandstone-mudstone contact to the middle of sandstones in fault blocks.

sandstones (Fig. 6).

Inside a fault block, the differences between the dissolution porosity and the distance from the source-connecting fault is not apparent within 1 m to the sandstone-mudstone contacts (Fig. 8C). Beyond 1 m from the sandstone-mudstone contacts, the dissolution porosity is relatively higher and has a negative relationship with the distance from the source-connecting fault (Fig. 8C).

### 4.3. Characteristics of fluid inclusions

Fluid inclusions formed during the diagenetic process of red-bed reservoirs are primarily of liquid-rich two-phase aqueous inclusions, which include inclusions occurring in quartz overgrowth and carbonate cements (mainly calcite and ankerite) and inclusions occurring in the annealed microfractures (AMF) in quartz grain (Fig. 12). The inclusions are relatively small, and the dimension is generally smaller than 10 μm (generally range from 2 to 8 μm); the gas-liquid ratios are usually less than 15%.

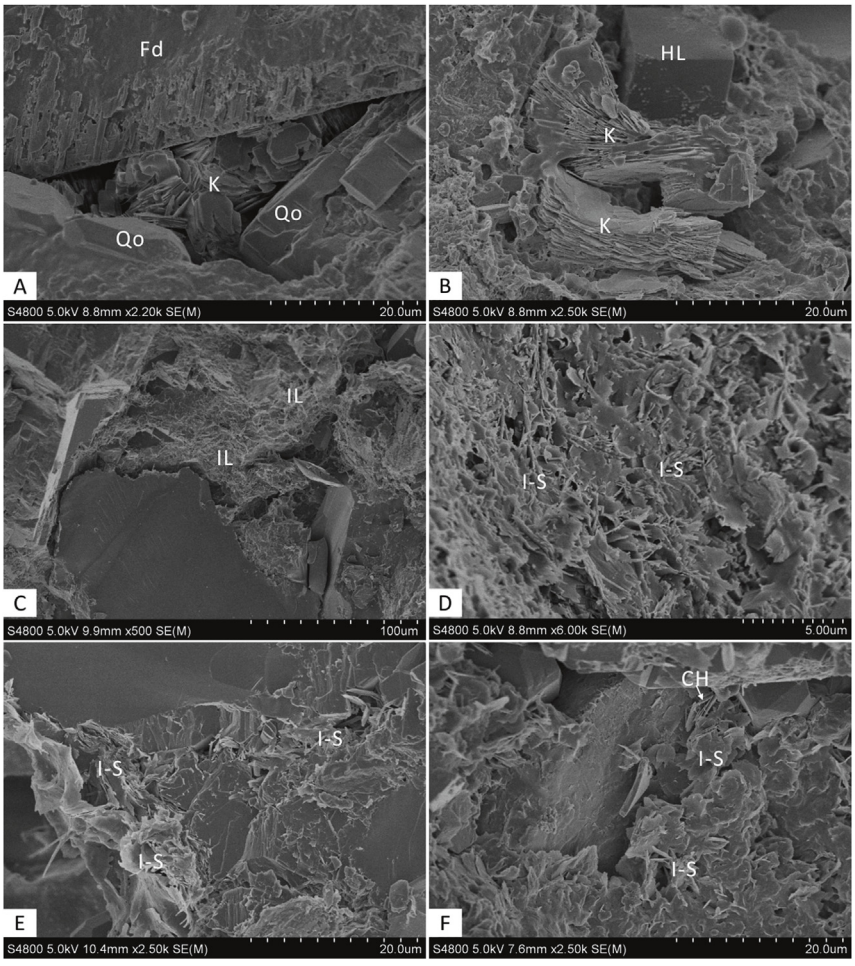


**Fig. 9.** Authigenic clay minerals in red-bed sandstone reservoirs of *Ek1-Es4x* in Dongying Depression. (A) Dissolution of feldspar, kaolinite and quartz overgrowth filling in intergranular pores from well Guan-113 at 2494.49 m; (B) Kaolinite and halite filling in intergranular pores from well Guan-120 at 2950.09 m; (C) Hair-like illite filling in intergranular pores from well Fs-1 at 3584.2 m; (D) Illite-smectite mixed layer minerals from well G-892 at 3065.9 m; (E) Illite-smectite mixed layer minerals from well Fs-1 at 3584.2 m; (F) Chlorite and illite-smectite mixed layer minerals from well F-151 at 2687.5 m. K-kaolinite; IL-illite; I-S-illite and smectite mixed layers; CH-chlorite; HL-halite.

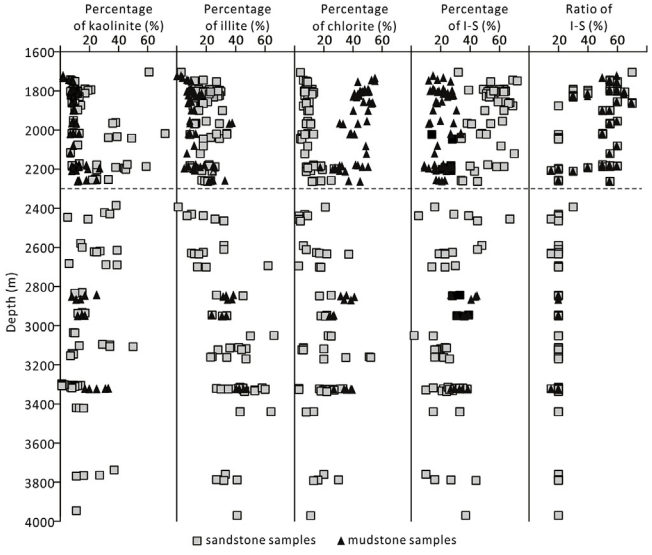


**Fig. 10.** The content and vertical distribution of clay minerals of red-bed sandstone reservoirs and mudstones of the lower Eocene *Ek1-Es4x* in the Dongying Depression.

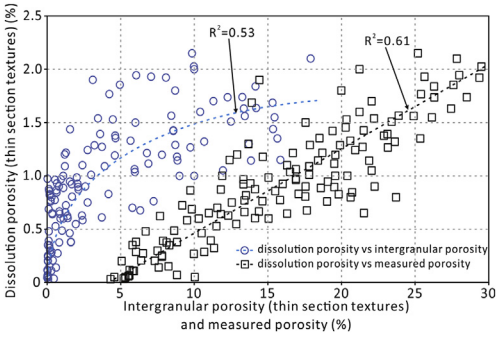


**Fig. 11.** Correlations between dissolution porosity (thin section textures) and the intergranular porosity (thin section textures) and the measured porosity.

The first ice melting temperatures are mainly between −26 °C and −20 °C, which indicates the composition of the inclusions can be modeled using the NaCl-$H_2O$ system. The last ice melting temperatures yield a range of salinities in terms of eq. wt% NaCl. The salinity and homogenization temperature distributions for all samples measured are shown in Fig. 13 and Fig. 14, respectively.

Salinity and homogenization temperature (Th) values of the inclusions in quartz overgrowths and of the inclusions in annealed microfractures have essentially the same range and distributions, suggesting that the trapping environments are broadly similar. However, these values contrast with the salinity and Th values of the inclusions trapped in the carbonate cements, indicating that they were formed under different diagenetic environments.

The homogenization temperature-salinity bivariate plots indicate that the aqueous inclusions in quartz overgrowths and AMF and carbonate cements can generally be divided into one or two groups (Fig. 15). For Sample A, both the aqueous inclusions in quartz overgrowth and AMF, and that in carbonate cements generally form two groups, the homogenization temperatures and the salinities of

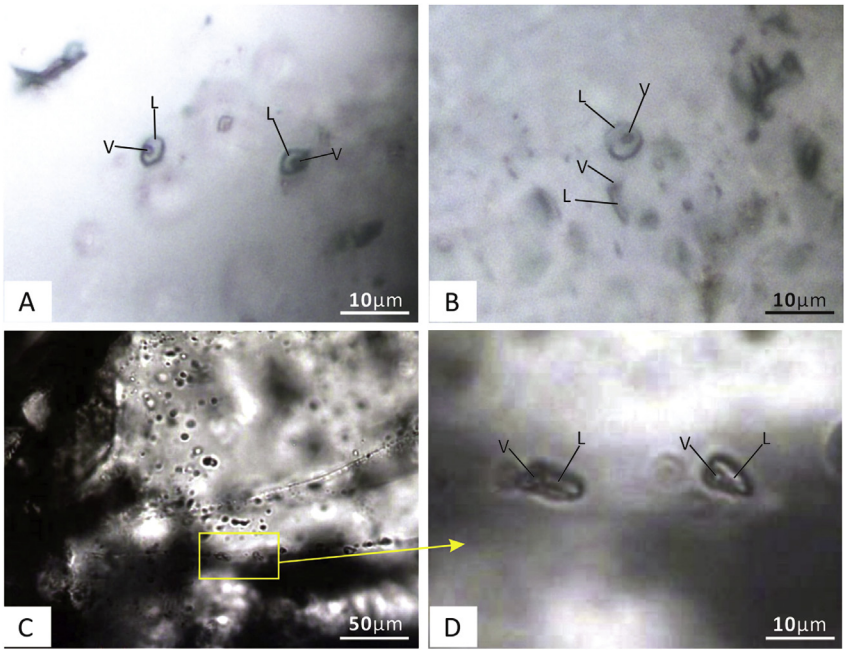


**Fig. 12.** Liquid-rich two-phase aqueous inclusions in quartz overgrowth and annealed microfractures in quartz grain of red-bed reservoirs in the Dongying Depression. (A) Primary liquid-rich two-phase aqueous inclusions in quartz overgrowth, Well Fs-1, 3584.2 m; (B) Primary liquid-rich two-phase aqueous inclusions in carbonate cement, Well Guan-113, 2494.49 m; (C) and (D) Primary liquid-rich two-phase aqueous inclusions in annealed microfractures in quartz grain, Well Fs-1, 3584.2 m.

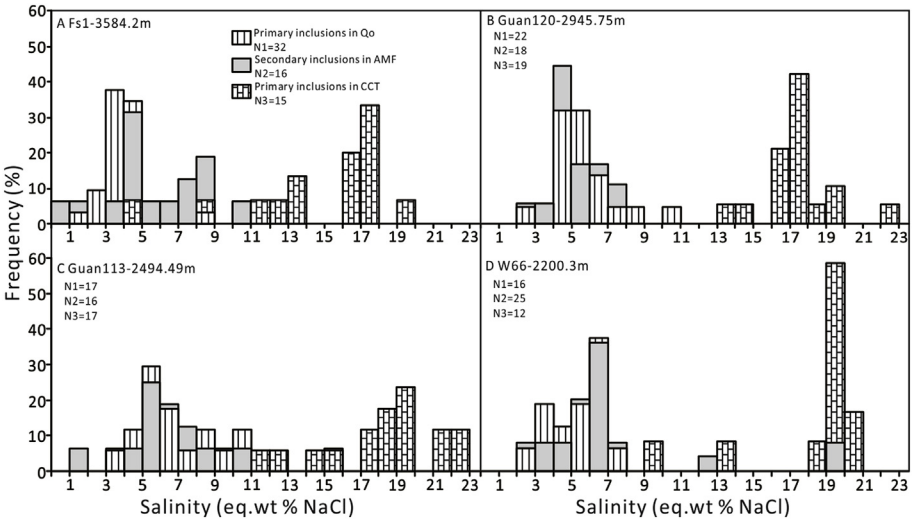


**Fig. 13.** Frequency distribution histograms showing salinities for liquid-rich two-phase aqueous inclusions in the four samples of red-bed reservoirs in the Dongying Depression. The histograms for the three inclusion types are superimposed since each type of inclusion is considered separately in determining the frequency. Salinities are given in weight percent NaCl equivalent on a NaCl-$H_2O$ basis. Qo-quartz overgrowth, AMF- annealed microfractures in quartz grain, CCT-carbonate cement.

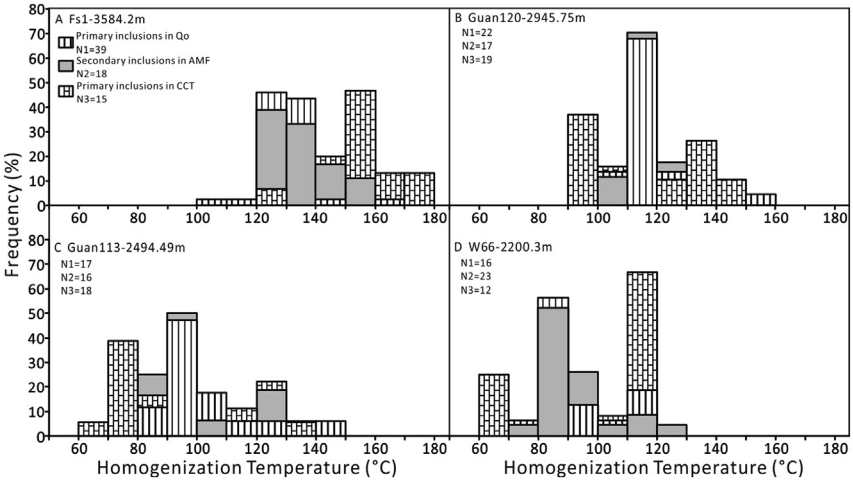


**Fig. 14.** Frequency distribution histograms showing homogenization temperatures for liquid-rich two-phase aqueous inclusions in the four samples of red-bed reservoirs in the Dongying Depression. The histograms for the three inclusion types are superimposed since each type of inclusion is considered separately in determining the frequency. All of the inclusions homogenize to liquid. Qo-quartz overgrowth, AMF-annealed microfractures in quartz grain, CCT-carbonate cement.

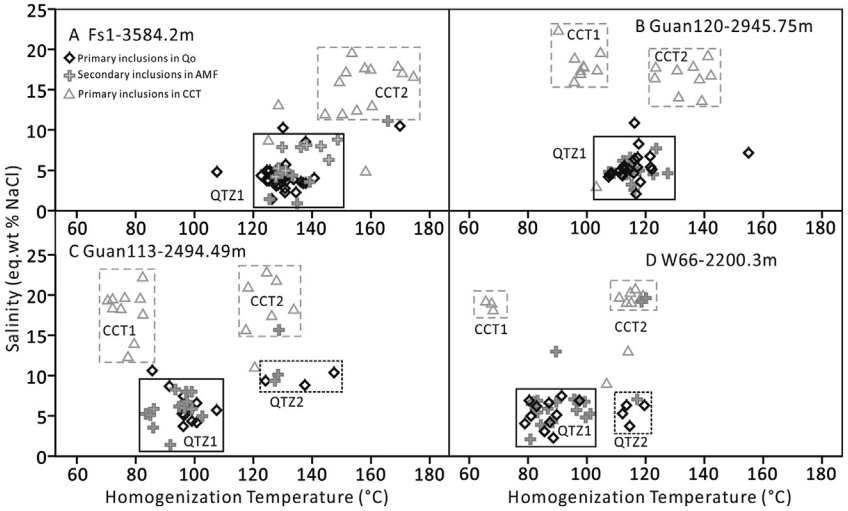


**Fig. 15.** Salinity vs. Homogenization temperature bivariate plots for the fluid inclusions trapped in quartz overgrowths, the AMF and in carbonate cements in the four samples from the red-bed reservoirs in the Dongying Depression. Qo-quartz overgrowth, AMF-annealed microfractures in quartz grain, CCT-carbonate cement.

inclusions in carbonate cements are higher than that of inclusions in quartz overgrowths and AMF (Fig. 15A). A minor group of inclusions in quartz overgrowths and AMF have higher Th values (Fig. 15A). In Sample B there are two groups of aqueous inclusions in carbonate cements and one group in quartz overgrowths and AMF. The Th values for inclusions in quartz overgrowths and AMF plot in the two groups defined by inclusions trapped in carbonate cements. The salinities of the latter two groups are higher than that of the inclusions in the quartz overgrowths and AMF (Fig. 15B). There are two groups defined by the data from the aqueous inclusions in quartz overgrowths and AMF, and also two groups defined by the fluid inclusions trapped in carbonate cements in the C and D samples. (Fig. 14C and D). The temperature gaps between the QTZ1 and QTZ2 groups of fluid inclusions in the same type of host minerals are usually more than 15 °C. The homogenization temperatures of the second group of inclusions in quartz overgrowths and AMF are close to or slightly higher than those of the second group in carbonate cements. The salinities of the inclusions in the carbonate cements are significantly higher than that of the inclusions in the quartz overgrowths and the AMF (Fig. 15C and D). Comparisons between the Th and salinity values and the relative positions of different groups of aqueous inclusions in the four samples indicate that the aqueous inclusions in the red-bed reservoirs can be divided into 4 groups i.e. QTZ1, QTZ2, CCT1 (mainly calcite in sandstone near the sandstone-mudstone contact), and CCT2 (mainly isolated ankerite and ferro-calcite in the center of sandstone). The four groups of aqueous inclusions indicate that the red-bed reservoirs may have experienced four diagenetic fluid stages each with different properties.

## 5. Discussion

### 5.1. Evolution of diagenetic fluids

Fluid inclusion microthermometric data is combined with: 1) the burial history (Fig. 16) and 2) relative formation sequences of the authigenic and diagenetic minerals in the red-bed reservoirs to produce a time framework which elucidates the trapping sequence of aqueous fluids. The geological time ranges of the four groups of fluid inclusions were established by the crossing of burial history curves and isotherms. Firstly, for a group of fluid inclusion, compare the homogenization temperatures with the isotherm to determine the range of this group of fluid inclusion on the corresponding burial history curve; secondly, the two ends of the temperature range on the burial history curve are projected on the time coordinates to obtain the beginning and ending of the entrapment of fluid inclusions; thirdly, the average values of the beginning and ending ages of the four groups of fluid inclusions in the four samples were calculated to represent the trapping timing for the four groups of fluid inclusions. Therefore the trapping time of each fluid inclusion group is as follows: QTZ1: 32.2–26.4 Ma, QTZ2: 15.1–0 Ma, CCT1: 35.7–32.2 Ma and CCT2: 26.4–21.4 Ma, respectively. The order of cementation from old to young is: CCT1, QTZ1, CCT2 and QTZ2, recording different diagenetic fluids by the red-bed sandstone reservoirs.

The red-bed deposition of the *Ek1-Es4x* in the Dongying Depression began at approximately 50 Ma (Qiu et al., 2004). No fluid inclusion recorded formation fluid activity prior to 37 Ma. The fluid inclusion homogenization temperature of CCT1 is relatively low, indicating precipitation during a shallow burial period of the reservoirs and thus recorded the characteristics of formation fluids in the early stage. The properties of the original sedimentary water directly affected the evolution of the formation or pore water, and thus the properties of the connate water controlled the diagenetic environments in the early stages (Alagarsamy et al., 2005; Carvalho et al., 2014; Zhang et al., 2014). During the deposition of *Ek1-Es4x*, the climate was arid, and the water circulation was restricted with concomitant deposition of clastic and evaporate (Wang et al., 2012a, 2015; Liu et al., 2017). The formation water was highly saline and strong alkaline (Tan et al., 2010; Li et al., 2013). During the burial process, compaction caused the originally absorbed water in mudstones to migrate into the adjacent sandstone units, forming high-salinity and alkaline diagenetic environments (Fig. 16).

The early diagenetic fluids during the burial of the reservoirs might have also been affected by clay-mineral dehydration in the interbedded mudstones. Because of the impact of relatively high paleogeothermal gradients, high lake water salinity, and strong alkaline fluids (Deconinck et al., 2014; Mefteh et al., 2014; Wang et al., 2016), kaolinite and smectite can be transformed rapidly to illite and chlorite in the mudstone interval. The low content of kaolinite, the high content of chlorite and the distribution of illite and ratio of I-S in the mudstones indicate that the timing and degree of transformation was quite early and high in the initial burial stage (Fig. 10). During the transformation process of clay minerals, a large number of metal cations, such as $Ca^{2+}$, $Na^{+}$, $Fe^{2+}$, $Mg^{2+}$ and $Si^{4+}$, may be produced (Bristow and Milliken, 2011; Wang et al., 2016, 2017b), and further increased the salinity of the fluids. The fluid inclusion data indicate that the role of the first-stage diagenetic fluid may be dated back to the initial deposition stage to 37 Ma (Fig. 16).

Biomarkers of the crude oil in red-bed sandstone reservoirs are characterized by distinct phytane advantage, high content of

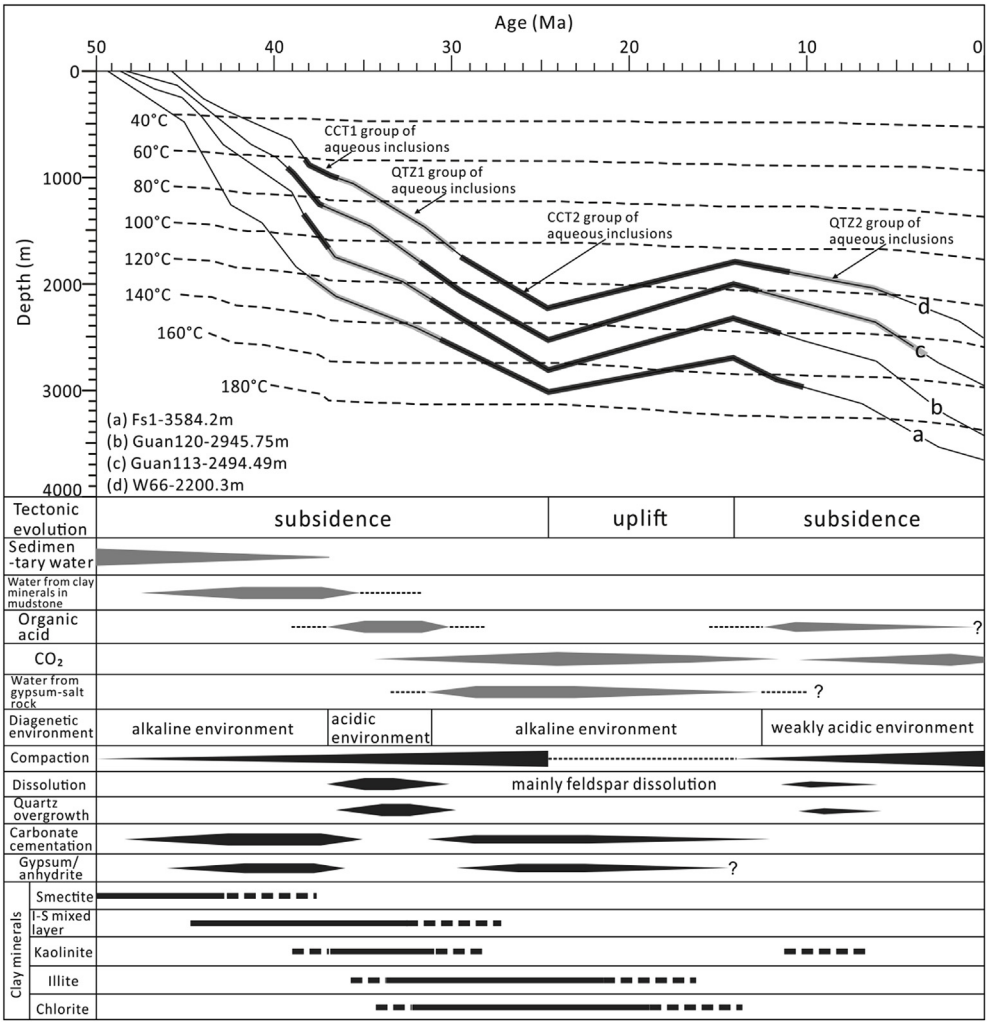


**Fig. 16.** The fluid sources, evolution of diagenetic fluids and environments and diagenetic sequence of red-bed reservoirs in the Dongying Depression. Temperatures were modeled by Hu et al. (2001) and burial history curves were modeled by Qiu et al. (2004).

gammaceranes, low content of 4-methylsteranes and rearranged steranes and anti-L shape distribution of C27, C28 and C29 steranes, which are consistent with the characteristics of *Es4s* hydrocarbon source rocks (Meng et al., 2011; Wang et al., 2012b). The crude oil in the red-bed sandstone reservoirs was derived from *Es4s* hydrocarbon source rocks, indicating a good hydrologic connection between the source rocks and the sandstones via fault conduits. The organic matter in the source rock is mainly of Type II (Jin et al., 2001). With increasing burial, the hydrocarbon source rocks in *Es4s* reached a temperature range of 80–120 °C between 38.1 Ma and 29.9 Ma, which is favorable for the production of organic acids and $CO_2$ (Surdam et al., 1984; Morad et al., 2000; Heydari and Wade, 2002; Prochnow et al., 2006). Abundant organic acids and $CO_2$ were released into the reservoirs, neutralizing the early alkaline fluids and developing an acidic diagenetic environment. The timing of this process (37–31.2 Ma) is essentially consistent with the timing of the fluid flow recorded by fluid inclusions in quartz overgrowths and AMF (Fig. 16). The salinity of the fluids recorded was primarily 3–7 eq. wt% NaCl. At this time, the transformation of clay minerals essentially ceased, and the impact of the diagenetic fluids from the interbedded mudstone on the sandstone reservoirs was limited.

With increasing burial, the organic acids began to dehydrate substantially through decarboxylation (Heydari and Wade, 2002; Prochnow et al., 2006), which caused the pH value of the fluid to increase gradually. In addition, gypsum began to thermally decompose substantially, releasing alkaline fluids rich in metal cations (Ma et al., 2016), which might have caused the formation fluids to gradually become alkaline. At the end of the *Ed* period, though the Dongying Depression underwent a regional tectonic uplift, the temperature was still within the range of decarboxylation of organic acid and thermal dehydration of gypsum. The formation fluid remained alkaline. The CCT2 group inclusions in the ferro-carbonates recorded the diagenetic fluids of this stage, which occurred primarily from 31.2 Ma to 11.5 Ma (Fig. 16). The salinity of fluids was generally of 10–22 eq. wt% NaCl.

During re-subsidence low volumes of organic acids might have migrated into the red-bed reservoirs along with oil emplacement. As the formation temperature increased, the content of organic acids in the formation fluids gradually declined, whereas the content and partial pressure of $CO_2$ would have gradually increased (Er-Raioui et al., 2002; Kribek et al., 2007; Beha et al., 2008), thus controlling the pH characteristics of the formation fluids in the late stage, causing the formation fluids to become weakly acidic. This acidic diagenetic fluid was recorded by the QTZ2 group fluid inclusions, trapped after 11.5 Ma (Fig. 16). The salinity of fluids was generally of 3–11 eq. wt% NaCl.

### 5.2. Diagenetic evolution of red-bed sandstone reservoirs

The red-bed sandstone reservoirs of the Dongying Depression experienced alternating acidic and alkaline diagenetic environments, which resulted in a series of diagenetic events in the reservoirs (Fig. 17).

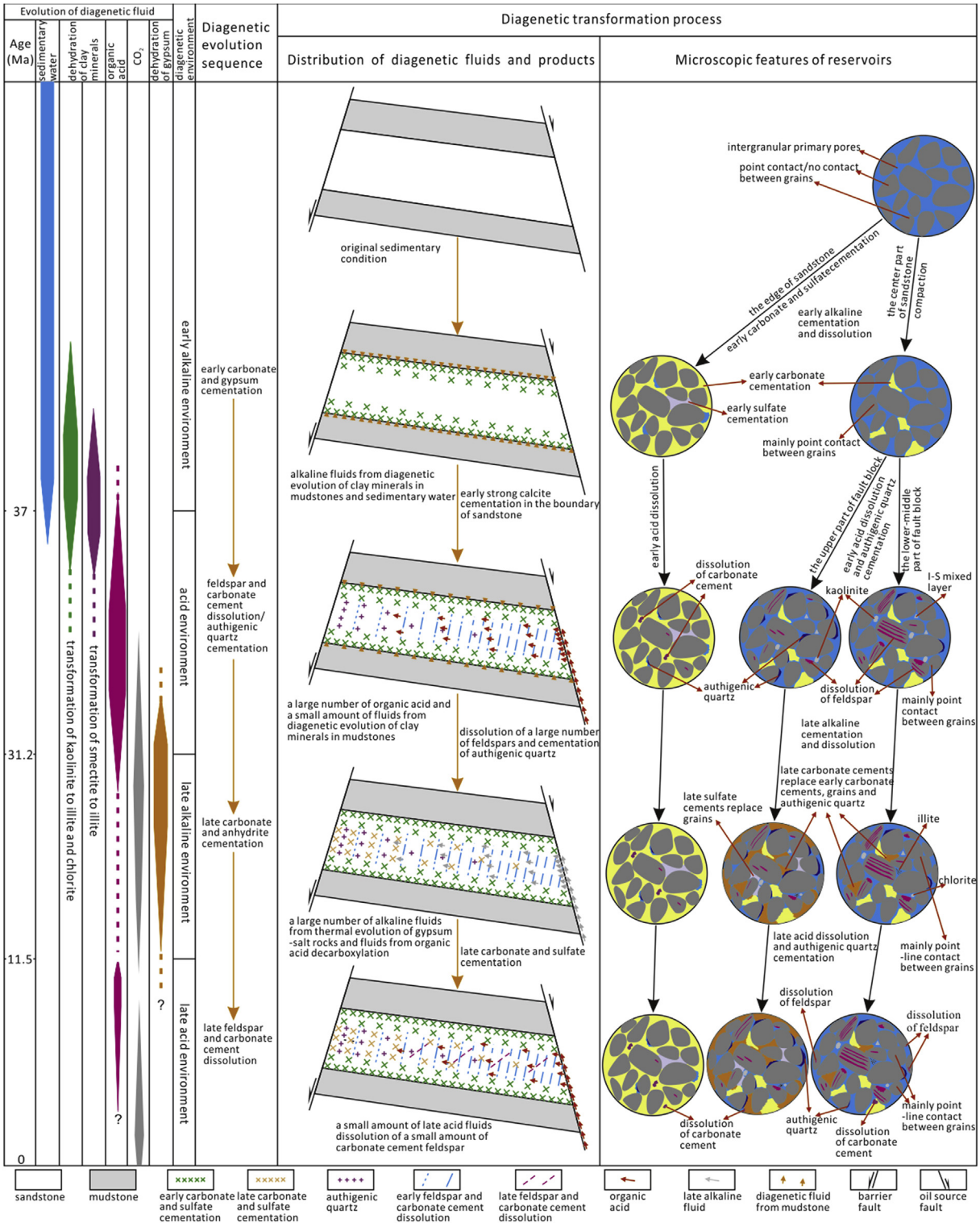


**Fig. 17.** Diagenetic environment, diagenetic sequence and diagenetic transformation process of red-bed reservoirs of the lower Eocene *Ek1-Es4x* in the Dongying Depression. There are significant differences in diagenetic evolution and diagenetic strength at different positions of sand bodies interbedded with mudstones in fault blocks.

The original depositional water and formation water affected by clay-mineral transformation within mudstones controlled the formation of the early alkaline diagenetic environments in the red-bed sand reservoirs before 37 Ma (Wang et al., 2016). The high-salinity alkaline fluids in the mudstones adjacent to the sandstone units triggered the development of strong cemented sandstones with calcite and gypsum along sandstone-mudstone contacts (Fig. 6A; Chen et al., 2009; Li et al., 2014; Wang et al., 2016). With the precipitation of cements, the salinity of the fluids gradually decreased, and the amount of cements decreased gradually from the sandstone-mudstone contacts to the center of sandstones (Fig. 4C; Milliken and Land, 1993; Dutton, 2008; Chen et al., 2009; Li et al., 2014; Wang et al., 2016, 2017a). Abundant primary intergranular pores were preserved in the middle part of sandstone units (Figs. 6B and 17).

From 37 Ma to 31.2 Ma, the organic acids released by the thermal evolution of hydrocarbon source rocks in *Es4s* had progressively converted the alkaline environment of the reservoirs to an acidic environment. After the fluid entered the sandstone reservoirs through faults in the lower part of the fault blocks, the tight cementation nature of the sandstones near the sandstone-mudstone contacts developed in the early stage made the acidic fluid more concentrated in the zone of intergranular pores in the center of the sandstones (Wang et al., 2016, 2017b), forming abundant feldspar dissolution pores, which gradually increased the amount of acidic dissolution pores from the sandstone-mudstone contacts to the center of the sandstones (Figs. 4F and 6). The higher the intergranular pore content is, the more favorable for organic acids to enter the reservoir would be, and thus producing more dissolution pores (Fig. 11). Because of the dissolution, the content of plagioclase is lower in the center part than that near the boundary of sandstones (Figs. 6 and 7C). That is why the content of kaolinite is close to zero near the boundary of sandstones while is high in the center part of sandstones (Fig. 6).

The dissolution of feldspar provided material sources for the cementation of quartz overgrowth and kaolinite during the period of 37 Ma to 31.2 Ma (Fig. 16). Other processes such as limited transmission distance of diffusion, lack of fluid source, amount, limited influencing range of compaction-driven flow and convection under burial environment, cannot adequately explain the distribution of feldspar dissolution pores and quartz overgrowth in the center part of sandstones in fault block (Bjørlykke, 1993, 1994; Bjørlykke and Jahren, 2012). Good hydrologic connections between the source rocks and the sandstones enabled acidic thermal fluids from the source to migrate into the reservoir sandstones through fault conduits (Wang et al., 2016). These acidic thermal fluids migrated from the sag belt to the gentle slope belt due to the locations of source rocks and sandstones (Wang et al., 2017b). The distribution of feldspar-dissolution pores and quartz overgrowth might correspond with the migration of acidic thermal fluids in fault blocks. When the acidic thermal fluids migrated from the lower part of the fault block (e.g., Well Guan-118 (2980–3050 m), Well W-135 (2260–2350 m)) to the upper part (e.g., Well Guan-120 (2900–3020), Well W-96 (1920–2240 m)), the dissolution capability became gradually weakened; some rich dissolution products (e.g., $SiO_2$) were simultaneously carried by the thermal fluids (Bjørlykke and Jahren, 2012), where they were precipitated in the upper part of the fault block to form authigenic quartz and other cements (Lu et al., 2013; Mork, 2013; Wang et al., 2017b). The dissolved minerals in the lower part of the fault block were transported out of the dissolution zone, causing a net increase in the porosity of the reservoirs there (Fig. 17).

From 31.2 Ma to 11.5 Ma, with an increase in the burial depth and temperature, the decarboxylation of organic acids and thermal evolution of gypsum-salt rocks released high-salinity alkaline water, which converted the formation fluids from acidic to strongly alkaline and developed an alkaline diagenetic environment in the late stage. Because the sandstones near the sandstone-mudstone contacts were tightly cemented in the early stage, the late alkaline fluids were confined to the center part of sandstones, which caused the precipitation of ferro-calcite and ankerite (Fig. 16), resulting in an increase of the amount of ferro-carbonate from the sandstone-mudstone contacts to the center of sandstones (Fig. 4D). During this period kaolinite and smectite were transformed to illite and chlorite rapidly (Figs. 10 and 16), which would provide ions for the precipitation of ferro-calcite and ankerite (Bristow and Milliken, 2011; Wang et al., 2016, 2017b). The migration of exogenetic thermal fluid might also be partly responsible for the distribution of carbonate cements in the center of sandstones in fault blocks (Figs. 8A and 17). Compared to calcite in sandstones near the sandstone-mudstone contacts, the precipitation temperature and depth of ferro-calcite and ankerite in the center of sandstones is higher and deeper (Fig. 5).

After 11.5 Ma, the diagenetic environment of the reservoirs gradually transformed from a strongly alkaline to a weakly acidic. This resulted in minor dissolution porosity of the feldspar and carbonate cements and quartz overgrowth in the late stage with similar distribution features (Figs. 16 and 17).

Compaction occurred throughout the entire diagenetic process. The early strong cementation in the sandstones near the sandstone-mudstone contacts inhibited compaction, resulting in a stronger compaction in the center of the sandstones.

### 5.3. Causes for the formation of high-quality reservoirs

The diagenetic evolution indicates that the alternating evolution of multiple alkaline and acidic diagenetic environments and the redistribution of diagenetic products in fault block are the controlling factors for the development of high-quality red-bed sandstone reservoirs.

The alternating evolution of multiple alkaline and acidic diagenetic environments controls the diagenesis of the reservoirs and distribution patterns of reservoir pores. The strong cementation under an alkaline diagenetic environment in the early stage controlled the distribution of acidic and alkaline formation fluids in the reservoirs in the late stage, which established the basis for the distribution features of diagenesis and reservoir pores in the reservoirs. Diagenesis in the sandstones near the sandstone-mudstone contacts is of a single type and is primarily the product of the alkaline environments in the early stage. In contrast, the middle part of the thick-layered sandstones exhibits a multi-phase superposition of alkaline cementation and acidic dissolution with cementation. Because of the alternating evolution of multiple alkaline and acidic diagenetic environments, the reservoir pores are therefore primarily distributed in the middle of the thick-layered sandstones, and are characterized by the coexistence of primary intergranular pores and acidic dissolution pores (Fig. 17). This explains why the porosity of the reservoir quality gradually improves from the sandstone-mudstone contacts to the center of sandstones (Fig. 6).

The distribution of diagenetic products promoted the differentiation of reservoir physical properties in the center part of the thick-layered sandstones inside fault blocks. The primary intergranular pores and dissolution pores were mainly developed at the lower part of fault blocks. The dissolution products and metal cations are precipitated in the upper part of fault blocks, forming authigenic quartz and carbonate cements in the late stage, filling primary and secondary pores, which further reduce the porosities of the reservoirs in the upper part of fault blocks.

The good spatial and temporal configurations between the various types of diagenetic events controls the development of lithological traps of diagenetic origin. After being constrained by formation water, the sandstones with carbonate tight cementation are prone to produce a water-lock effect in which high capillary pressure forms, which turns the corresponding sandstone layers into virtual cap layers (Mallon and Swarbrick, 2008; Wang et al., 2011; Liu et al., 2012). Relative high porosity is preserved in the center part of sandstones; such reservoirs would have good hydrocarbon accumulations. Because of the distribution features of diagenetic products, lithological traps of diagenetic origin of a certain size are therefore developed in the red bed sandstone reservoirs of the Dongying Depression. For example, a high-production well segment in *Ek1* (a daily oil production of 5.75 t) that was successfully drilled in the Boxing Sag of Well G-94 was located in the middle of a thick-layered sandstone in the lower part of a fault block (Fig. 18; Liu et al., 2011).

## 6. Conclusions

The lower Eocene red-bed reservoirs in the Dongying Depression evolved through an early-stage alkaline diagenetic environment, followed by an acidic diagenetic environment, then a late-stage alkaline diagenetic environment and finally, a late-stage acidic diagenetic environment. The red-bed sandstone reservoirs experienced multiple types of diagenesis, including compaction, carbonate cementation,

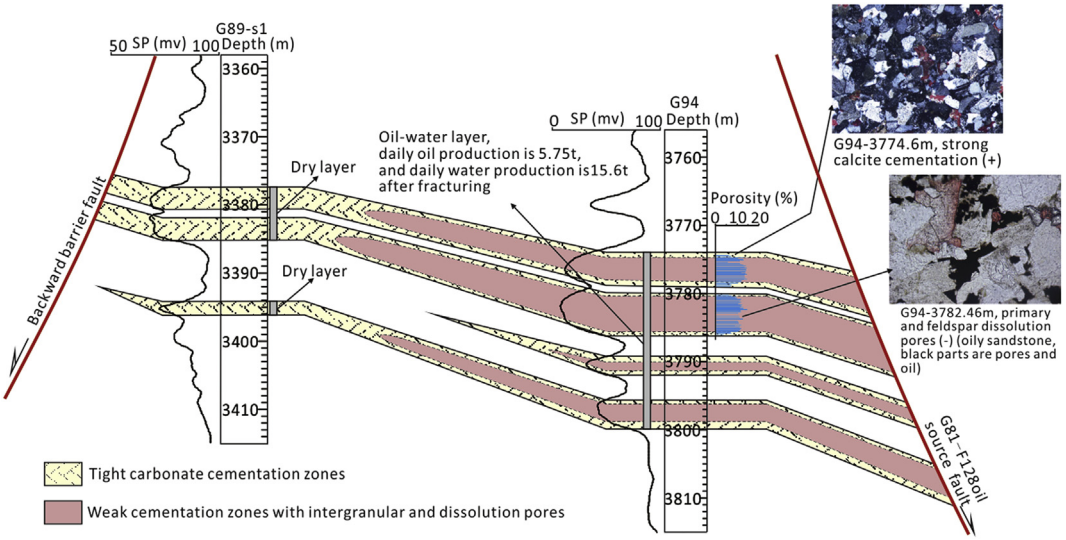


**Fig. 18.** Diagenetic traps of red-bed reservoirs in the section crossing Well G-94 and G-89-s1 in the Dongying Depression. The section location as in Fig. 1B.

gypsum and ankerite cementation, feldspar and carbonate dissolution, quartz overgrowth cementation, clay minerals cementation and transformation. Due to the impact of the early-stage alkaline diagenetic environment, there was strong cementation of calcite and gypsum in the sandstones near the sandstone-mudstone contacts. From the sandstone-mudstone contact to the center of sandstones, cementation becomes rapidly weakened and abundant intergranular pores were preserved in the middle of thick-layered sandstone units. The influence of acidic formation fluids caused a large number of dissolution pores in the feldspar and carbonate cements, forming synchronous occurrence of primary intergranular pores and acidic dissolution pores. From the middle part of sandstone units to the sandstone-mudstone contacts, dissolution becomes weakened gradually and the percentage of ferrocarbonate decreased. Migration of exogenetic thermal fluids may be responsible for the gradual waning of dissolution and the progressive enhancement of cementation from the lower part to the upper part of fault blocks. The effects of alternating evolution of multiple alkaline and acidic diagenetic environments and the distribution of diagenetic products caused the development of high-quality red-bed reservoirs in the center part of the thick-layered sandstones in the lower part of fault blocks. Because of the temporal and spatial relationships between the diagenetic stages and their products, lithological traps of a diagenetic origin developed in the red-bed reservoirs.

## Acknowledgments

This work was co-funded by the National Nature Science Foundation of China (Grant No. U1762217, Grant No. 41402095), the Fundamental Research Funds for the Central Universities (Grant No. 18CX05027A), the National Science and Technology Special of China (Grant No. 2017ZX05009001), Strategic Priority Research Program of the Chinese Academy of Sciences (Grant No. XDA14010301), and the Scientific and Technological Innovation Project (Grant No. 2015ASKJ01) Financially Supported by Qingdao National Laboratory for Marine Science and Technology (Grant No. 2015ASKJ01). Thanks are also expressed to the Geosciences Institute of the Shengli Oilfield, SINOPEC, for permission to access their in-house database, providing background geologic data and permission to publish the results.

## References

Aagaard, P., Jahren, J., 2010. Special issue introduction: compaction processes - porosity, permeability and rock properties evolution in sedimentary basins. Mar. Petrol. Geol. 27, 1681–1683.

Al Gahtani, F., 2013. The influence of diagenetic alterations on porosity in the Triassic Narrabeen group, southern Sydney basin, Australia. Geol. Q. 57, 613–628.

Alagarsamy, R., Wolff, G.A., Chester, R., 2005. Partitioning and speciation of trade metal diagenesis in differing depositional environments in the sediments of the Oman Margin. Aquat. Geochem. 11, 195–213.

Beard, D.C., Weyl, P.K., 1973. Influence of texture on porosity and permeability of unconsolidated sand. AAPG Bull. 57, 349–369.

Beha, A., Thomsen, R.O., Littke, R., 2008. Thermal history, hydrocarbon generation and migration in the Horn Graben in the Danish North Sea: a 2D basin modelling study. Int. J. Earth Sci. 97, 1087–1100.

Besly, B.M., Turner, P., 1983. Origin of red beds in a moist tropical climate (Etruria Formation, Upper Carboniferous, UK). Geol. Soc. Spec. Publ. 11, 131–147.

Bjørlykke, K., 1993. Fluid flow in sedimentary basins. In: In: Cloetingh, S., Sassi, W., Horvath, F., Puigdefabregas, C. (Eds.), Basin Analysis and Dynamics of Sedimentary Basin Evolution. Sediment. Geol, vol. 86. pp. 137–158.

Bjørlykke, K., 1994. Fluid-flow processes and diagenesis in sedimentary basins. Geol. Soc. Spec. Publ. 78, 127–140.

Bjørlykke, K., Jahren, J., 2012. Open or closed geochemical systems during diagenesis in sedimentary basins: constraints on mass transfer during diagenesis and the prediction of porosity in sandstone and carbonate reservoirs. AAPG Bull. 96, 2193–2214.

Bristow, T.F., Milliken, R.E., 2011. Terrestrial perspective on authigenic clay mineral production in ancient Martian lakes. Clay Clay Miner. 59, 339–358.

Carvalho, A.S.G., Dani, N., De Ros, L.F., Zambonato, E.E., 2014. The impact of early diagenesis on the reservoir quality of pre-salt (aptian) sandstones in the Espirito Santo Basin, Eastern Brazil. J. Petrol. Geol. 37, 127–141.

Chen, D., Pang, X., Jiang, Z., Zeng, J., Qiu, N., Li, M., 2009. Reservoir characteristics and their effects on hydrocarbon accumulation in lacustrine turbidites in the Jiyang Super-depression, Bohai Bay Basin, China. Mar. Petrol. Geol. 26, 149–162.

Deconinck, J.F., Crasquin, S., Bruneau, L., Pellenard, P., Baudin, F., Feng, Q., 2014. Diagenesis of clay minerals and K-bentonites in late permian/early Triassic sediments of the Sichuan basin (chaotian section, Central China). J. Asian Earth Sci. 81, 28–37.

Dill, H.G., Khishigsuren, S., Melcher, F., Bulgamaa, J., Bolorma, K., Botz, R., Schwarz-Schampera, U., 2005. Facies-related diagenetic alteration in lacustrine–deltaic red beds of the Paleogene Ergeliin Zoo Formation (Erdene Sum area, S. Gobi, Mongolia). Sediment. Geol. 181, 1–24.

Dubiel, R.F., Smoot, J.P., 1994. Criteria for interpreting paleoclimate from red beds: a tool for Pangean reconstructions. In: Embry, A.F., Beauchamp, B., Glass, B.J. (Eds.), Pangea: Global Environments and Resources. Canadian Society of Petroleum, Calgary, pp. 295–310.

Dutton, S.P., 2008. Calcite cement in Permian deep-water sandstones, Delaware Basin west Texas: origin, distribution, and effect on reservoir properties. AAPG Bull. 92, 765–787.

Er-Raioui, H., Bouabdelli, M., Belayouni, H., Chellai, H., 2002. Basin geodynamics and thermal evolution of organic material: example from the Qasbat-Tadla Basin, central Morocco. J. Afr. Earth Sci. 32, 605–618.

Feng, Y., Li, S., Lu, Y., 2013. Sequence stratigraphy and architectural variability in late Eocene lacustrine strata of the Dongying depression, Bohai Bay basin, eastern China. Sediment. Geol. 295, 1–26.

Folk, R.L., 1974. Perology of Sedimentary Rock. Hemphill Publishing Co, Texas.

Folk, R.L., 1980. Petrology of Sedimentary Rocks. Hemphill Publishing, Austin, Texas, pp. 182.

Hammer, E., Mork, M.B.E., Naess, A., 2010. Facies controls on the distribution of diagenesis and compaction in fluvial-deltaic deposits. Mar. Petrol. Geol. 27, 1737–1751.

Henares, S., Caracciolo, L., Cultrone, G., Fernández, J., Viseras, C., 2014. The role of diagenesis and depositional facies on pore system evolution in a Triassic outcrop analogue (SE Spain). Mar. Petrol. Geol. 51, 136–151.

Heydari, E., Wade, W.J., 2002. Massive recrystallization of low-Mg calcite at high

temperatures in hydrocarbon source rocks: implications for organic acids as factors in diagenesis. AAPG Bull. 86, 1285–1303.
Hu, S., O'Sullivan, P.B., Raza, A., Kohn, B.P., 2001. Thermal history and tectonic subsidence of the Bohai Basin, northern China: a Cenozoic rifted and local pull-apart basin. Phys. Earth Planet. In. 126, 221–235.
Jiang, Z., Liu, H., Zhang, S., Su, X., Jiang, Z., 2011. Sedimentary characteristics of large-scale lacustrine beach-bars and their formation in the Eocene Boxing sag of Bohai Bay basin, east China. Sedimentology 58, 1087–1112.
Jiang, Z., Liu, L., 2011. A pretreatment method for grain size analysis of red mudstones. Sediment. Geol. 241, 13–21.
Jin, Z., Sun, Y.Z., Yang, L., 2001. Influences of deep fluids on organic matter of source rocks from the Dongying depression, East China. Energy Explor. Exploit. 19, 479–486.
Kent, D.V., Opdyke, N.D., 1978. Paleomagnetism of the Devonian Catskill red beds: evidence for motion of the coastal New England-Canadian Maritime region relative to cratonic north America. J. Geophys. Res. 83, 4441–4450.
Kribek, B., Sykorova, I., Pasava, J., Machovic, V., 2007. Organic geochemistry and petrology of barren and Mo-Ni-PGE mineralized marine black shales of the Lower Cambrian Niutitang Formation (South China). Int. J. Coal Geol. 72, 240–256.
Lampe, C., Song, G., Cong, L., Mu, X., 2012. Fault control on hydrocarbon migration and accumulation in the Tertiary Dongying depression, Bohai Basin, China. AAPG Bull. 96, 983–1000.
Li, J., Song, G., Gao, Y., Yang, X., 2013. Recovery of the paleosedimentary environment in Eocene red formations and its geological significances for Dongying Sag. Pet. Geol. Oilfield Dev. Daqing 32, 43–48 (in Chinese with English abstract).
Li, Q., Jiang, Z., Liu, K., Zhang, C., You, X., 2014. Factors controlling reservoir properties and hydrocarbon accumulation of lacustrine deep-water turbidites in the Huimin Depression, Bohai Bay Basin, East China. Mar. Petrol. Geol. 57, 327–344.
Li, Z., Chen, J.S., Guan, P., 2006. Scientific problems and frontiers of sedimentary diagenesis research in oil-gas-bearing basins. Acta Petrol. Sinica. 22, 2113–2122.
Liu, C., Han, H., Liu, S., 2011. Sedimentary Characteristics, Oil Accumulation and Exploration Practice of Red Beds in the Jiyang Subbasin. Geosciences Institute of the Shengli Oilfield, SINOPEC Internal reports (in Chinese).
Liu, C., Zheng, H., Hu, Z., Yin, W., Li, S., 2012. Characteristics of carbonate cementation in clastic rocks from the Chang 6 sandbody of Yanchang Formation, southern Ordos Basin. Sci. China Earth Sci. 55, 58–66.
Liu, J., Wang, J., Cao, Y., Song, G., 2017. Sedimentation in a continental high-frequency oscillatory lake in an arid climatic background: a case study of the lower Eocene in the Dongying depression, China. J. Earth Sci. 28, 628–644.
Lundegard, P.D., 1992. Sandstone porosity loss-a "big picture" view of the importance of compaction. J. Sediment. Petrol. 62, 250–260.
Lu, P., Fu, Q., Seyfried, W.E., Hedges, S.W., Soong, Y., Jones, K., Zhu, C., 2013. Coupled alkali feldspar dissolution and secondary mineral precipitation in batch systems–2: new experiments with supercritical $CO_2$ and implications for carbon sequestration. Appl. Geochem. 30, 75–90.
Ma, B., Cao, Y., Eriksson, K.A., Jia, Y., Wang, Y., 2016. Burial evolution of evaporites with implications for sublacustrine fan reservoir quality: a case study from the Eocene Es4x interval, Dongying depression, Bohai Bay Basin, China. Mar. Petrol. Geol. 76, 98–114.
Mallon, A.J., Swarbrick, R.E., 2008. Diagenetic characteristics of low permeability, non-reservoir chalks from the Central North Sea. Mar. Petrol. Geol. 25, 1097–1108.
MacDonald, A.J., Spooner, E.T.C., 1981. Calibration of a Linkam TH 600 programmable heating-cooling stage for microthermometric examination of fluid inclusions. Econ. Geol. 76, 1248–1258.
Marriott, S.B., Morrissey, L.B., Hillier, R.D., 2009. Trace fossil assemblages in upper Silurian tuff beds: evidence of biodiversity in the old red sandstone of southwest Wales, UK. Palaeogeogr. Palaeocl. 274, 160–172.
Mefteh, S., Medhioub, M., Essefi, E., Jamoussi, F., 2014. Effect of diagenesis on clay mineralogy and organic matter in the Tunisian southern subsurface. J. Geol. Soc. India 83, 198–210.
Meng, J., Liu, L., Jiang, Z., Wang, Y., Gao, Y., Liu, S., 2011. Geochemical characteristics of crude oil and oil-source correlation of the Paleogene "red bed" in the south slope of the Dongying depression, Bohai Bay basin, China. Energy Explor. Exploit. 29, 397–413.
Milliken, K.L., Land, L.S., 1993. The origin and fate of silt sized carbonate in subsurface Miocenee Oligocene mudstones, south Texas Gulf Coast. Sedimentology 40, 107–124.
Morad, S., Al-Aasm, I.S., Nader, F.H., Ceriani, A., Gasparrini, M., Mansurbeg, H., 2012. Impact of diagenesis on the spatial and temporal distribution of reservoir quality in the Jurassic Arab D and C members, offshore Abu Dhabi oilfield, United Arab Emirates. Geoarabia 17, 17–56.
Morad, S., Ketzer, J.M., De Ros, L.F., 2000. Spatial and temporal distribution of diagenetic alterations in siliciclastic rocks: implications for mass transfer in sedimentary basins. Sedimentology 47, 95–120.
Mork, M.B.E., 2013. Diagenesis and quartz cement distribution of low-permeability Upper Triassic-Middle Jurassic reservoir sandstones, Longyearbyen $CO_2$ lab well site in Svalbard, Norway. AAPG Bull. 97, 577–596.
Nguyen, B.T.T., Jones, S.J., Goulty, N.R., Middleton, A.J., Grant, N., Ferguson, A., Bowen, L., 2013. The role of fluid pressure and diagenetic cements for porosity preservation in Triassic fluvial reservoirs of the Central Graben, North Sea. AAPG Bull. 97, 1273–1302.
Parcerisa, D., Gómez-Gras, D., Travé, A., Martín-Martín, J.D., Maestro, E., 2006. Fe and Mn in calcites cementing red beds: a record of oxidation-reduction conditions: examples from the Catalan Coastal Ranges (NE Spain). J. Geochem. Explor. 89, 318–321.
Paxton, S.T., Szabo, J.O., Ajdukiewicz, J.M., Klimentidis, R.E., 2002. Construction of an intergranular volume compaction curve for evaluating and predicting compaction and porosity loss in rigid-grain sandstone reservoirs. AAPG Bull. 86, 2047–2067.
Prochnow, E.A., Remus, M.V.D., Ketzer, J.M., Gouvea, J.C.R., de Souza, R.S., De Ros, L.F., 2006. Organic-inorganic interactions in oilfield sandstones: examples from turbidite reservoirs in the Campos Basin, offshore eastern Brazil. J. Petrol. Geol. 29, 361–379.
Qiu, N., Li, S., Zeng, J., 2004. Thermal history and tectonic-thermal evolution of the Jiyang depression in the Bohai Bay basin, east China. Acta Geol. Sin. 78, 263–269 (in Chinese with English abstract).
Quan, C., Liu, Z., Utescher, T., Jin, J., Shu, J., Li, Y., Liu, Y., 2014. Revisiting the Paleogene climate pattern of East Asia: a synthetic review. Earth Sci. Rev. 139, 213–230.
Retallack, G.J., 1991. Miocene Paleosols and Ape Habitats of Pakistan and Kenya. Oxford University Press, New York.
Schmid, S., Worden, R.H., Fisher, Q.J., 2004. Diagenesis and reservoir quality of the Sherwood sandstone (Triassic), corrib field, Slyne basin, west of Ireland. Mar. Petrol. Geol. 21, 299–315.
Schoner, R., Gaupp, R., 2005. Contrasting red bed diagenesis: the southern and northern margin of the Central European Basin. Int. J. Earth Sci. 94, 897–916.
Sheldon, N.D., 2005. Do red beds indicate paleoclimatic conditions?: A Permian case study. Palaeogeogr. Palaeocl. 228, 305–319.
Surdam, R.C., Boese, S.W., Crossey, L.J., 1984. The chemistry of secondary porosity. In: In: Surdam, R.C., McDonald, D.A. (Eds.), Clastic Diagenesis. AAPG Memoir, vol. 37. pp. 127–149.
Tan, X., Tian, J., Li, Z., Zhang, S., Wang, W., 2010. Diagenesis evolution of fragmental reservoir in alkali sediment environment: taking the Member 4 of Shahejie Formation of steep-slope zone in Dongying sag, Shandong, China for example. Geol. Bull. China 29, 535–543 (in Chinese with English abstract).
Turner, P., 1980. Continental Red Beds. Elsevier, Amsterdam, pp. 562.
Turner, P., Archer, R., 1977. The role of biotite in the diagenesis of red beds from the Devonian of northern Scotland. Sediment. Geol. 19, 241–251.
Udden, J.A., 1914. Mechanical composition of clastic sediments. GSA Bull. 25, 655–744.
Van Houten, F.B., 1973. Origin of red beds a review: 1961–1972. Annu. Rev. Earth Planet Sci. 1, 39–61.
Walker, T.R., 1967. Formation of red beds in modern and ancient deserts. GSA Bull. 78, 353–368.
Walker, T.R., 1974. Formation of red beds in moist tropical climates: a hypothesis. GSA Bull. 85, 633–638.
Walker, T.R., 1976. Diagenetic origin of continental red beds. In: Faulke, H. (Ed.), The Continental Permian in Central, West, and South Europe. Riedel Publishing, Dordrecht, pp. 240–282.
Walker, T.R., 1981. Nature and origin of hematite in the Moenkopi Formation (Triassic), Colorado Plateau: a contribution to the origin of magnetism in red beds. J. Geophys. Res. 86, 317.
Wang, J., Cao, Y., Liu, H., Gao, Y., 2012a. Characteristics of sedimentary environment and filling model of the lower submember of the fourth member of Shahejie Formation, Dongying Depression. Acta Sedimentol. Sin. 30, 274–282 (in Chinese with English abstract).
Wang, J., Cao, Y., Liu, H., Gao, Y., 2015. Formation conditions and sedimentary model of over-flooding lake deltas within continental lake basins: an example from the Paleogene in the Jiyang Subbasin, Bohai Bay Basin. Acta Geol. Sin. 89, 270–284.
Wang, J., Cao, Y., Liu, K., Liu, J., Xue, X., Xu, Q., 2016. Pore fluid evolution, distribution and water-rock interactions of carbonate cements in red-bed sandstone reservoirs in the Dongying Depression, China. Mar. Petrol. Geol. 72, 279–294.
Wang, J., Cao, Y., Liu, K., Liu, J., Muhammad, K., 2017a. Identification of sedimentary-diagenetic facies and reservoir porosity and permeability prediction: an example from the Eocene beach-bar sandstone in the Dongying Depression, China. Mar. Petrol. Geol. 82, 69–84.
Wang, J., Cao, Y., Song, G., Liu, H., 2017b. Diagenetic evolution and formation mechanisms of high-quality reservoirs under multiple diagenetic environmental constraints: an example from the Paleogene beach-bar sandstone reservoirs in the Dongying depression, Bohai Bay basin. Acta Geol. Sin. 91, 232–248.
Wang, Y., Liu, L., Meng, J., Jiang, Z., Gao, Y., Liu, S., 2012b. Oil-source correlation study of the Paleogene red beds in the Boxing sag of the Dongying depression, eastern China. Rev. Mex. Ciencias Geol. 29, 725–734.
Wang, P., Yang, R., Liu, W., Chen, S., Li, C., 2011. Reservoir characteristics and favorable area prediction of Devonian Kizirtag formation in Bashituo area, Tarim Basin. Energy Explor. Exploit. 29, 575–596.
Wei, Q., Yuan, X., 2008. Sediment features and oil-gas pool forming regularity of red beds in the eastern China oilfields. Acta Petrol. Sin. 29, 191–194 (in Chinese with English abstract).
Wilson, M.E.J., Wah, E.C.E., Dorobek, S., Lunt, P., 2013. Onshore to offshore trends in carbonate sequence development, diagenesis and reservoir quality across a land-attached shelf in SE Asia. Mar. Petrol. Geol. 45, 349–376.
Wentworth, C.K., 1922. A scale of grade and class terms for clastic sediments. J. Geol. 30, 377–392.
Yamashita, I., Surinkum, A., Wada, Y., Fujihara, M., Yokoyama, M., Zaman, H., Otofuji, Y., 2011. Paleomagnetism of the middle-late Jurassic to cretaceous red beds from the peninsular Thailand: implications for collision tectonic. J. Asian Earth Sci. 40, 784–796.
Zhang, Y., Kaiser, K., Li, L., Zhang, D., Ran, Y., Benner, R., 2014. Sources, distributions, and early diagenesis of sedimentary organic matter in the Pearl River region of the South China Sea. Mar. Chem. 158, 39–48.